Syracuse University

# SURFACE

January 2017

# DEVELOPMENT OF A LOCALIZED ELECTROCHEMICAL PROPERTIES TEST METHOD : A STUDY OF CoCrMo AND Ti ALLOY LOCALIZED ELECTROCHEMICAL BEHAVIOR

Sile Hu
*Syracuse University*

## Recommended Citation

**Abstract:** Corrosion of metallic biomaterials in biomedically-relevant environments depends on the local physical and chemical structure of the metal surface at the metal-solution interface, and the geometry of the electrode system.   Local surface structure, including defects, inclusions, and grain boundaries may locally alter the electrode behavior, while local geometries, including crevice-like geometries or small electrode areas will give rise to specific changes in electrochemical behavior. Methods to detect local defects or surface flaws electrochemically may be possible with the appropriate combination of microelectrodes and pipette geometries. In order to have a better understanding of the localized electrochemical behavior under given conditions, a localized electrochemical impedance spectroscopy (LEIS) technique was developed and evaluated along with standard polarization testing. CoCrMo and Ti samples were tested using this technique and under varying conditions to simulate small areas, and the presence of crevice-like geometries. The reference and counter electrodes were positioned within a small-diameter pipette tube with varying cross sectional diameters and varying heights from the working electrode surface.   In addition, two conditions were examined with solution both inside and outside of the pipette or with solution only on the inside. These conditions were selected to approximate different electrode conditions, surfaces and geometries relevant to medical device surfaces. Significant differences in both impedance and polarization behavior were seen with this local electrode system depending on the absence or presence of external solution, the diameter of the pipette, the distance of the pipette from the working electrode surface and the materials tested.

The polarization resistance of the working electrode for both Ti and CoCrMo decreased, and the corrosion current increased with increasing pipette cross sectional area (i.e., electrode

area) when no external solution was present. In the external solution condition, $E_{corr}$ of

CoCrMo samples became more negative and $R_{p,}$(the polarization resistance from the Tafel

fitting result) also decreased with increasing exposed area, while the $I_{corr}$ was not affected; for

Titanium, the value of $E_{corr}$, $I_{corr}$, and $R_p$ changed relatively little compared to the behavior in

the no-electrolyte-covered condition.

The impedance behavior of this electrode system was affected by the presence of

external solution or not.   In the no-external-electrolyte condition, the response behaved

according to a constant phase element Randles circuit with increasing area increasing the

capacitance (CPE-T) for both CoCrMo and Titanium, while the polarization resistance $R_p$

value for both CoCrMo and Titanium sample decreased. With external solution present, the

impedance behavior followed a crevice corrosion model proposed by Swaminathan and

Gilbert. Increasing the internal area, caused decreases in both internal pipette resistance ($R_o$)

and crevice resistance ($R_{cr}$) for both Titanium and CoCrMo samples, while the internal

capacitance ($CPE_o$) increased, and external capacitance ($CPE_{oc}$) as well as external surface

resistance ($R_{oc}$) changed relatively little compared to other parameters. In the external solution

case, the distance between the microelectrode and the sample surface caused the crevice

resistance, $R_{cr,}$ to decrease exponentially as distance increased. There is a critical distance

which leads to a sudden $R_{cr}$ value drop.

# DEVELOPMENT OF A LOCALIZED ELECTROCHEMICAL PROPERTIES TEST METHOD：A STUDY OF CoCrMo AND Ti ALLOY LOCALIZED ELECTROCHEMICAL BEHAVIOR

By

Sile Hu

B.E Biomedical Engineering,

Jinan University, China 2013

Thesis

Submitted in partial fulfillment of the requirements for the

Degree of Master of Science in Bioengineering

Syracuse University

May 2017

# ACKNOWLEDGEMENTS

# TABLE OF CONTENTS

# CHAPTER 1

# INTRODUCTION

The application of metallic biomaterials for therapeutic purposes can be tracked back centuries. At present, stainless steel (e.g., 316LSS), titanium based alloys (e.g., Ti-6Al-4V), CoCr alloys (e.g., CoCrMo) are the most widely used metallic biomaterials in all orthopedic and cardiovascular surgery applications. 316L stainless steel is one of the most commonly applied metallic materials from cardiovascular to otorhinology applications. CoCrMo alloys are typically applied to high wear resistance situations like artificial joints. Titanium alloys are favored for their great corrosion resistance, high biocompatibility and mechanical properties.

Even though these metallic biomaterials have excellent mechanical and biological properties, implant material failures can and do still occur prior to the implant design lifetime, as has been reported in vivo [1-4]. Due to the hostile body environment surrounding metallic implant materials, corrosion reactions caused by anodic and cathodic reactions result in interactions of the implant metal with the biological system. The interaction of implant material and the host biological surroundings cause the degradation of the implant which contributes to biological reactions such as inflammatory reactions, osteolysis, stress shielding and pain in the implant location, etc. [5-8] . Degradation of metallic biomaterials is usually the consequence of electrochemical reactions, wear or the combination of the two. Corrosion damage on implant surface can result in many different changes in structure, chemistry and local electrochemical properties.

Implant failure can be related to many factors other than corrosion. For example, processes like wear and fretting may lead to tribocorrosion, resulting in disruption of the oxide film and the release of the reactive metal ions from the surface. Also, electrochemical processes may include generalized corrosion, uniformly affecting the entire surface of the implant, and localized corrosion, affecting either regions of the device that are shielded from the tissue fluids (crevice corrosion) or seemingly random sites on the surface (pitting corrosion). Electrochemical and mechanical processes (stress corrosion cracking, corrosion fatigue, and fretting corrosion) may also interact, causing premature structural failure and accelerated release of metal particles and ions.[9]

Fretting and fatigue are the most common mechanically assisted corrosion types that are found in implant applications. Pitting is also of concern in some alloys including stainless steel and NiTi alloys. Fretting-crevice corrosion is one of the typical mechanically assisted corrosion (MAC) mechanisms seen in implants, and this corrosion behavior has been shown in many retrieved implants [10, 11]. Brown et al. indicated that fretting corrosion contributes to the initiation of modular interface corrosion, such as crevice corrosion behavior. [12] The occurrence of fretting corrosion can result in localized wear as well as initiate fatigue cracks which likely reduce the fatigue strength of implant materials and leads to biocompatibility concerns [13, 14] Usually fretting corrosion occurs at the interface of two different phases (e.g. different metals at the interface of the hip implant modular taper

junction), the micromotion between the two surfaces result in a disruption of the passive oxide film, resulting in the acceleration of a small scale local surface corrosion. Crevice corrosion may be associated with fretting corrosion and depending on many factors such as metal combination, solution type, crevice size, etc.[15, 16]

Surface oxide films present on metallic materials not only contributes to corrosion resistance but also to tissue compatibility. To limit the further oxidation, these oxide films on the metal surface are usually compact, non-porous, highly abrasion resistant and atomically structured to limit the ions and electrons transferring from metal oxide – solution interface. The electrochemical characteristics of oxide-covered surfaces are relatively stable if the oxide film condition remains unchanged. The potential established by the electrochemical reactions at a metal surface immersed in a solution is called the Open Circuit Potential (OCP) or corrosion potential ($E_{corr}$). Due to the thermodynamic force and the chemical activity of the metal, there are electrochemical reactions occurring at the surface of the metal-solution interface, which leads metals to corrode. When the system maintains electronic neutrality, the rate of oxidation and the rate of reduction would be equal when the system is at its open circuit potential, and the system is "at equilibrium".

Oxide films may be disrupted mechanically leading to metal ion release and oxide film reformation.   These reactions result in electrode potential drops and can impact on the local environmental surroundings. For instance, the oxide film formed

on CoCrMo alloy is predominantly $Cr_2O_3$. The valance of Cr ion might alter from $Cr^{3+}$ to $Cr^{6+}$ depending on the electrode potential. The release of these heavy metal ion species might have a negative impact (allergy, inflammation, etc.) on the host [17-19].

Once the oxide films are disrupted, the electrochemical balance of the metal-solution interface will be upset, leading to a drop in the OCP of the electrode. In addition, during mechanically assisted crevice corrosion, changes in solution chemistry inside the crevice can be significant due to the generation of hydrogen ions and the presence of chloride ions (resulting in a pH drop). An aggressive localized condition can be established that is significantly different than present outside of the crevice. There have been several studies of this type of corrosion behavior [11, 20-24]. These include efforts to improve the crevice corrosion behavior in hip implant. Gilbert et al,.[25] developed a thin polymer based self-reinforced composite SRC film made from PEEK, the PEEK fibers had been melted spin under the proper thermal and flow conditions to result in a highly oriented polymer structure that will impart significantly improved mechanical properties to the polymer. The SRC-PEEK films generated from this method can then be used as the interposing polymer layer between modular taper components. Also many other efforts had been made to generally prevent implant corrosion. Implant modification, for instance, is a common approach to improve the corrosion resistance, surface texture, wear resistance and biocompatibility of the metallic material [26-29]. Gerhard et al., [27] developed a method for producing a corrosion-inhibiting coating on an implant having a surface

and made of a bio corrodible magnesium alloy, the corrosion-inhibiting coating provided by this method causes a temporary inhibition, but not complete suppression, of the corrosion of the material in a physiological environment.

Techniques and test methods have been developed to obtain a better understanding of the mechanisms of implant corrosion. The most commonly-used test methods to systematically study the electrochemical behavior of a given alloy interacting with certain electrolyte are open circuit potential test (OCP), potentiodynamic polarization test and Electrochemical Impedance Spectroscopy (EIS). The general EIS method uses a classic three-electrode system to apply a small amplitude sinusoidal voltage as an input and measure the corresponding output current through the working electrode. Electrical analog models such as Randles' circuit are applied to fit the result and to interpret the capacitance and resistance of the test subject based on the frequency-dependent characteristic behavior.

The impedance of a metallic biomaterial surface can be affected by many factors such as exposed electrode area, electrode geometry, localized corrosion processes, immersion time, pH, etc.[30-32] However, with classic surface electrochemical test methods like EIS, it is hard to separate out the contributions of the corrosion reactions to the overall impedance spectra because the data is the average impedance over all exposed area while the degradation is typically a localized event.
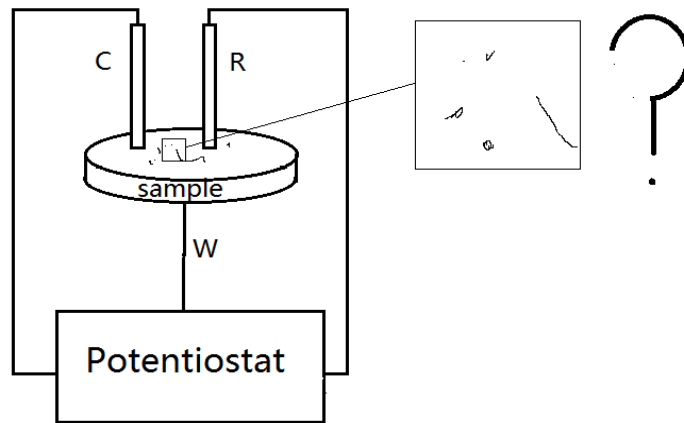
Overall measurement VS local variations

The development of localized electrochemical test methods is not new. Several technics had been developed to measure the localized impedance behavior[33-35]. These include the scanning droplet cell microscopy (SDCM)[36], scanning vibrating electrode technique(SVET)[37] and alternating current scanning electrochemical microscopy (AC-SECM)[38] are the most commonly techniques that use small electrodes immersed in the electrolyte closely approaching to sample to achieve the localization measurement. SDC uses a compact peristaltic pump to force electrolyte through a small diameter tube and into a specifically designed head. This SDC head is machined to allow electrolyte to flow past an installed Reference Electrode and then to a port at the base of the head. The SVET uses a single wire to measure voltage drops in solution. This voltage drop is a result of local current at the surface of a sample. Measuring this voltage in solution images the current at the sample surface. Current can be naturally occurring from a corrosion or biological process, or the current can be externally controlled using a galvanostat. However, how factors like

crevice geometries, small electrode areas and presence or absence of external electrolyte solution would influence the localized electrochemical behavior still cannot be studied with the techniques above.

While damaged regions of implant have been studied in terms of volume of material lost (using topographic methods), and by using qualitative and quantitative imaging methods to describe the damage modes, chemical changes and debris generation, there have been no direct methods developed to date to assess local alterations in the electrochemical properties of the surface. The ability to locally analyze changes in the electrochemical properties (e.g., potential, impedance, etc.) of an implant surface may add important new information into how in vivo corrosion affects implant surface performance.

However, in order to study local electrochemical properties, especially impedance behavior, methods need to be developed that are easy and well characterized to describe local properties. The effects of the test system on the response of the test are also important so that the responses seen can be properly interpreted.

In addition, the test system to be developed may serve as a model for the impedance performance of other implant geometries that include crevices or restricted solution geometry conditions. Finally, the method to be develop may be capable of

presenting localized regions with altered local solution chemistry, and focused

electrical fields to simulate localized corrosion conditions that may be representative

of the biological system.

Therefore, my work focused on development of the local electrochemical test

system, how the test system behaves under different conditions (with and without

external solution, with close proximity and with distance away from the surface of

interest, etc.) and how exactly these different conditions influence the localized

electrochemical behavior of CoCrMo and Ti alloy samples.

In this study, a new localized electrochemical impedance spectroscopy (LEIS)

system is developed. This test system is able to perform microelectrochemical

analysis on common biomaterials. The tests described can be performed rapidly, are

simple to use and are able to analyze different locations as well as variable crevice

geometries.

# CHAPTER 2

# RESEARCH GOAL AND INSTRUMENTATION DESIGN

## 2.1 Research Motivation and Goals

Metallic biomaterial corrosion in biomedically – relevant environments depends on the local physical and chemical structure of the metal surface at the metal-solution interface. Specifically, factors such as the alloy species at the surface, the structure and chemical properties of the surface as well as the presence and behavior of its oxides significantly influence the behavior of the alloy under corrosion conditions.
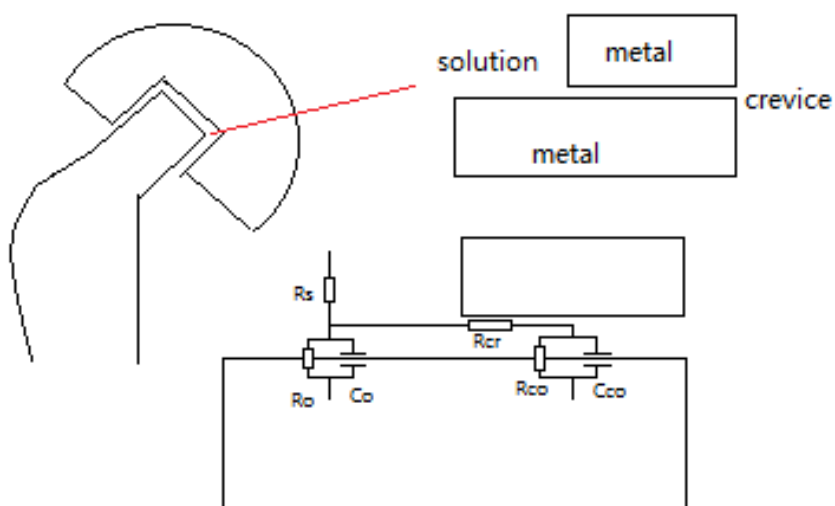


**Figure 2.1** Crevice model in modular taper junction

The surface oxide film on the metal and its electrochemical behavior can vary widely based on the amount of the alloy species present in the oxide, the inclusion size, distribution and density, and the defect density in the oxides. The area of the surface exposed to the electrolyte may also impact when and how the local corrosion occurs. When the sample area exposed decreases, the probability of the detecting an

area that contains a defect also decreases and the electrochemical response from that region of the sample will be more relevant to the presence or absence of defects. In another words, if the region analyzed is small, the region may consist mostly of defected surface, or will consist of non-defect containing surface. As the result, the electrochemical response of the surface should be more variable depending on the differences in structure present. The presence or absence of external electrolyte solution might also influence the electrochemical behavior locally.

In order to study and evaluate the localized electrochemical performance of metal-solution surfaces in different geometries (wire, rod, tube or sheet), a microelectrochemical test method which is able to sample controlled areas of a surface for the electrochemical response is needed. This approach should be able to apply microelectrode techniques, general electrochemical test technics (including OCP measurements, potentiodynamic polarization and impedance analysis) and an ability to spatially move and position the microelectrode rapidly and precisely on a surface for analysis.

Thus, several elements of this technique need to be defined:

1. The exposed condition (area, solution type and amount, the distance between sample and electrodes, etc.) of the sample should be controlled;

2. The method should be applicable for the various sample geometries (tube, slice, sheet, wire, etc);

3. The method should be able to perform systematic tests (OCP measurements, potentiodynamic polarization and impedance analysis);

4. The method should be able to move rapidly to detect any random region on the sample.

To fulfill the above requirements, the goals of this the study were to develop and assess test methods which are able to perform microelectrochemical analyses on common biomaterials. The tests should be rapid, simple and be able to analyze different locations as well as variable areas. The surface geometries to be investigated include flat sheet, single wire, tubes, segments of stents and whole segments of stents, and include the assessment of crevice-like geometries.

The tests will evaluate the performance of the system under varying conditions that include: with or without external solution present, varying pipette electrode area and working electrode-pipette distance.

## 2.2 Aims and Test System Design

The basic concept of the mini-electrode impedance test method is to place the reference and counter electrodes of a potentiostatic three-electrode system into a small pipette with electrolyte inside. This small pipette can then be brought into close contact with the surface of interest and the local region within the pipette diameter will be locally assessed. The region outside of the pipette can either contain solution or not. If it does not, then only the region being wetted will contribute to the signal and local behavior can be assessed. If the outside also has fluid, that fluid can be different than the internal solution and/or the location of the pipette (proximity to the surface, tightness of the seal between the pipette and sample, etc.) may all have effects on the electrochemical response.

The aims of the study are:

1.  Develop microelectrode probe which is capable of testing small regions of the sample (or controlling the detecting area size) to identify and quantitatively measure the variations in electrochemical properties. Additionally, the probe should be able to fit on various geometries (sheet, tube, wire and stent). At present stage the samples were made as sheet for start.

2.  Perform systematic tests (OCP measurements, potentiodynamic polarization and

    impedance analysis) in such small areas of varying electrochemical character on

    CoCrMo and Ti samples to determine the relationships between overall

    electrochemical response and local electrochemical variations.


In aim 1, a quantitative positioning system was used for precision microelectrode placement. The system, originally designed for micromechanical testing, has been modified to accommodate a scanning microelectrode system and electrode sample (see Fig. 2.2).
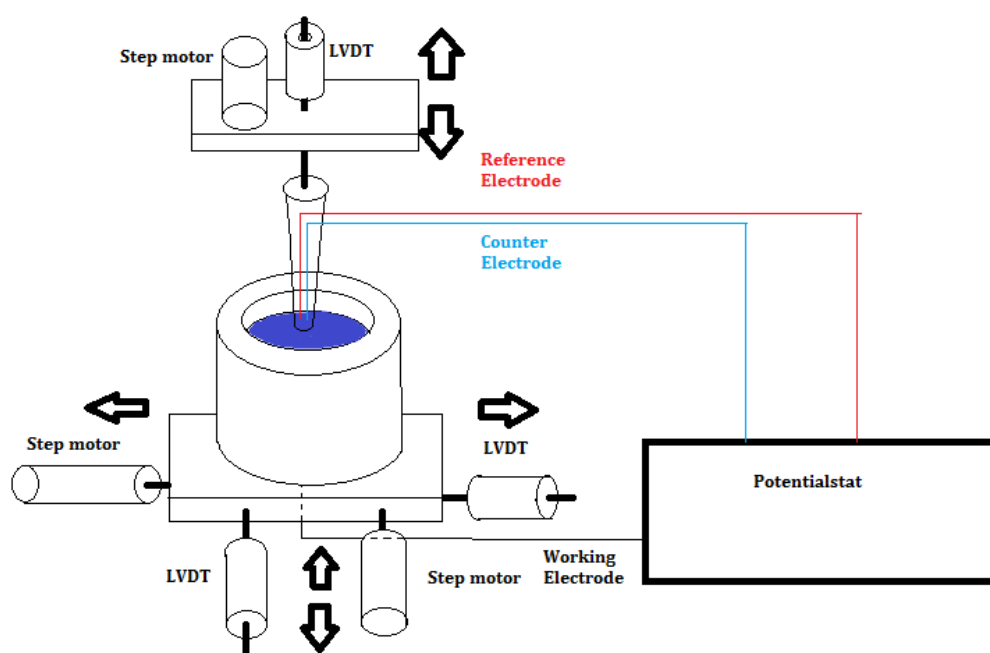


**Figure 2.2** System design sketch


The system is powered by a potentiostat and controlled by a Visual Basic/National Instruments-based program. The electrode probe positioning system was controlled and driven by a linear variable differential transformer (LVDT) sensor

paired with a DC motor connected to a multiaxial stage. With the accurate monitoring

of the position with the LVDT, every movement of the DC motor is precisely

calibrated down to 50 nm accuracy.

The electrode probes are made of pipette heads with different opening diameters

from a radius of 0.4 mm to 1.6 mm (see Fig. 2.5). The reference electrode is made of

silver wire (0.5 mm radius) coated with silver chloride, and the counter electrode was

made of pure platinum wire (0.5 mm radius). The reference electrode is calibrated

with standard silver chloride electrode before every test.
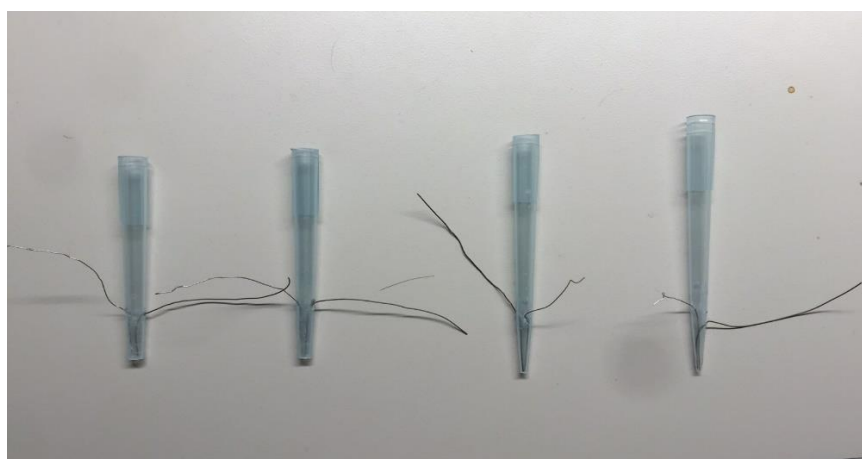


**Figure 2.5** Photograph of microelectrode probes.

In the preliminary study the sample holder was designed and made for the sheet

sample (see Fig. 2.6).
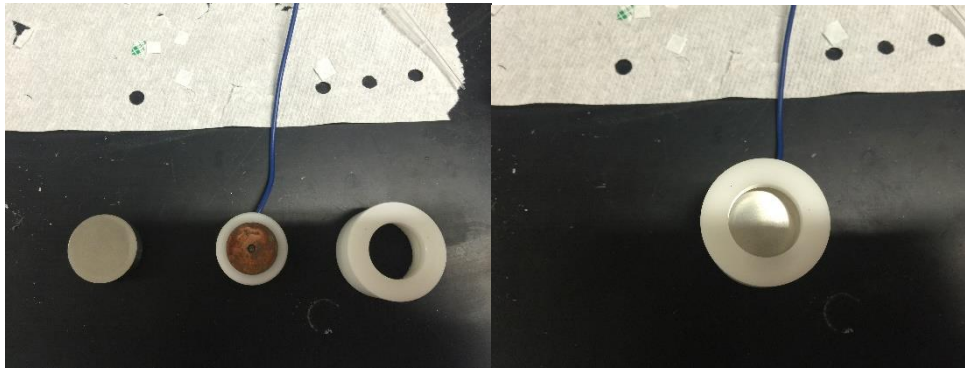
**Figure 2.6** Photographs of the typical sheet sample holder.

The other geometries sample holder was designed and will be developed in the future (see Fig. 2.7).



Tube/wire sample
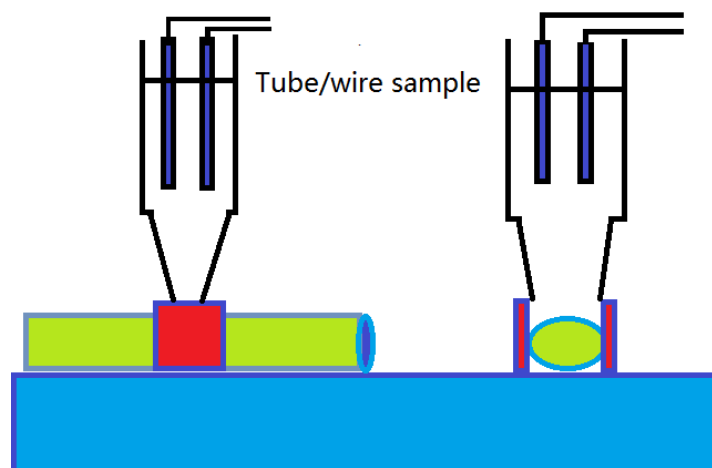
**Figure 2.7** Alternate geometry sample holder designs.

In general, with the microelectrode probes (with reference and counter electrodes) connected to the positioning system, relatively small regions of the sample are able to be investigated and tested repeatedly by moving the probe (see Fig. 2.8).
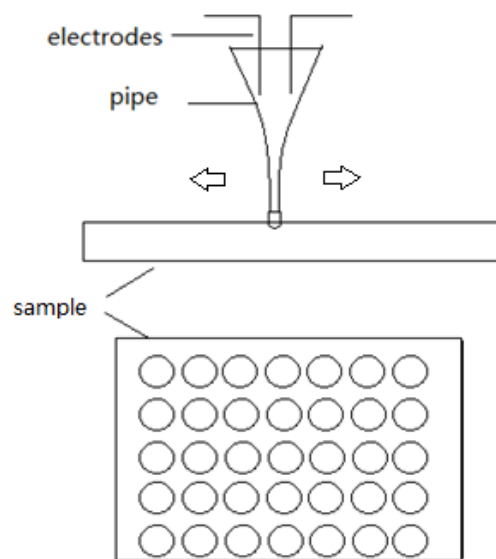
**Figure 2.8** Microelectrode scaning method.

In aim 2, a Solartron 1280C electrochemical test system was connected to the microelectrode probe to perform general electrochemical properties test such as open circuit potential measurement, potentiodynamic polarization test and electrochemical impedance spectroscopy. The data was collected using Corrware™ and ZPlot™. Cobalt chromium and titanium samples were selected for assessing the microelectrode system as well as investigating the local electrochemical behavior of typical metallic biomaterials.

# CHAPTER 3

# EXPERIMENTAL DESIGN AND MEASUREMENT

The goal of these experiments was to assess the capability of the designed

microelectrode system to perform general systematic electrochemical tests in a

relatively small area. Also, the local corrosion as well as crevice corrosion behavior of

CoCr and Ti sample associated with **A** (sample area exposed to solution), **d** (distance

between sample surface and pipette opening) were investigated.
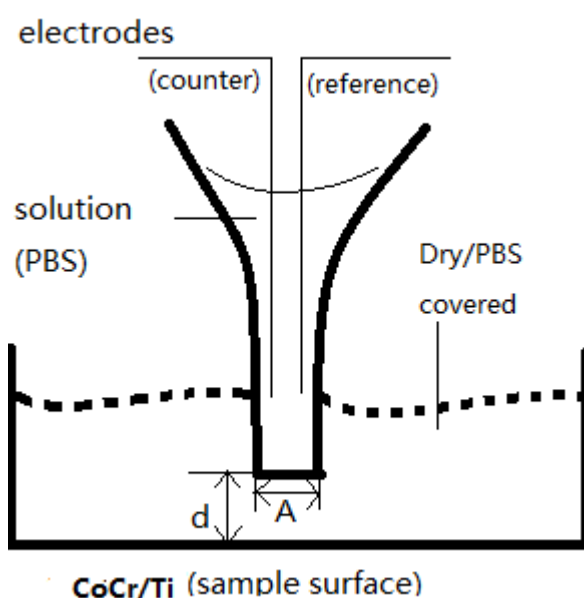


**Figure 3.1** A schematic of the microelectrode test set up for localized analysis of

electrochemical behavior. The set up consists of an electrode tip of varying opening

area (A), and sample distance, d. It can have solution over the entire sample, or just at

the electrode tip.

In these experiments, the main focus was on understanding the effects of the

parameters of the test on the electrochemical response of CoCrMo and Ti. Three

electrochemical methods were explored including open circuit potential

measurements, potentiodynamic polarization tests, and electrochemical impedance spectroscopy tests. The test parameters explored include the cross-sectional area of the pipettes, the pipette-sample surface distance, and the effect of the presence or absence of solution external to the pipette. These parameters were chosen for study in part to understand the role of these geometry elements, but also to simulate the internal versus external behavior of crevice-like geometries generated by the pipette-sample interaction.

The pipette area ranged from 0.5 to 8.0 mm$^2$, while the pipette-sample surface distance was controlled with a precision micrometer used to adjust the vertical location.   For solution in the pipette only, no external solution was placed, and only the solution within the pipette which made contact with the sample surface determined the electrode area.   This was governed primarily be surface tension effects and the diameter of the pipettes.   The vertical distance started with the pipette in contact and under a small amount of compressive load and was then displaced away from the surface with the micrometer to up to 1000 um away from the surface.

While not the focus of the present study, the configuration evaluated here may also have different internal and external solution chemistries present to explore the effects of differential solution on the local corrosion behavior.

## 3.1 Open circuit potential

**Specimens:**

The CoCrMo (ASTM F-1537) and titanium alloy (Ti-6Al-4V) premade sheet specimens were mechanically mirror polished by using wet emery paper through 600 grit followed by alumina suspension in water polish with 1 um, and immersed with 0.154M PBS for 1 hour (for stable oxide film generation), then washed by deionized water and ethanol. After wiping off the liquid drops with lens paper, the specimen was placed into a sample holder. The microelectrodes were injected with about 1 ml of 0.154 M PBS as the electrolyte.

**Measurement:**

The CoCr sheet specimen was placed into the sample holder and then attached to the positioning system. The microelectrodes were connected to the potentiostat (Solatron 1280C, Scribners Associates, USA) electrochemical system to measure the potential signals.

Initially, the no external electrolyte condition was tested where the microelectrodes were fully pressed onto the sample surface, and the OCP was measured for 30 mins. Then PBS was placed externally to the pipette and the OCP test was repeated. Then, a different pipette area was attached and a new area of the

surface was tested as above. This was repeated across all pipette areas tested. Three

trials for each pipette area (with and without external solution) were tested for

statistical comparison of the results.

## 3.2 Potentiodynamic polarization test

**Measurement:**

The parameters explored in these experiments were the pipette area and the presence or absence of external solution. The test set up was identical to that described for the OCP measurements.

Potentiodynamic polarization testing was performed by first bringing the sample surface to -0.7 V vs chloride Ag wire quasi-reference (Ag-wire) electrode and scanning at 2 mV/s to 0.2 V vs Ag-wire reference. These potential limits were chosen to minimize any major disruption to the oxide film and allowed for repeated testing on a single sample surface.

For the no-electrolyte-covered condition, the microelectrodes were fully pressed down onto the sample surface and the voltage versus current plots were captured. The polarization test was repeated for the fully immersed condition. Then the pipette was changed (different exposed area) from 0.4 mm radius to 1.6 mm radius and the polarization tests were repeated (both with and without external solution present).

The $I_{corr}$ and $E_{corr}$ were determined from the resulting data. $E_{corr}$ was determined as the potential where the current transited from cathodic to anodic during the scan,

and $I_{corr}$ was found from the Tafel approximation using the corrosion software. Three

trials were performed for each pipette area and material.

## 3.3 Electrochemical Impedance Spectroscope

**Specimens:**

The samples were prepared as they were for the above OCP and polarization tests.

**Measurement:**

In these experiments, both the area, **A** (pipette area), and the pipette-sample vertical distance, **d** were systematically varied.

The EIS tests applied a 10 mV sinusoidal potential at open circuit potential over a range of frequencies from 0.01 Hz to 20000 Hz.

For the no-electrolyte-covered condition, the microelectrodes were fully attached to the sample surface and the impedance was measured.   For the case of external solution present, the microelectrodes were fully pressed onto the sample surface and the impedance measured.   Then the pipette was shifted up 100 μm and the test repeated.   This sequence was repeated for each 100 μm step up to 1000 μm. Then the pipette was changed to a different exposed area from 0.4 mm radius to 1.6 mm radius and each test repeated. These tests were repeated three times.

**Analysis of EIS results:**

For electrochemical impedance spectroscopy tests, significantly different responses were observed between no external solution and the presence of external

solution. Thus, different equivalent circuit models were used to analyze the results

from each group of experiments.

For the no-external-electrolyte condition, the equivalent circuit model used was a

Randles circuit model, as shown below. This circuit was modified to have a constant

phase element (CPE) replace the capacitor since non-ideal impedance response was

observed [39]. The elements of the model include Ro, the surface oxide resistance (or

low frequency resistance), C (or CPE) the capacitive or constant phase element, and

Rs, the solution resistance.   Each of these elements of the model are hypothesized to

be affected by the factors of pipette area and the distance of the pipette from the

surface. Extrinsic (non-area dependent) and intrinsic (area-normalized) measurements

of these parameters were determined in these experiments.
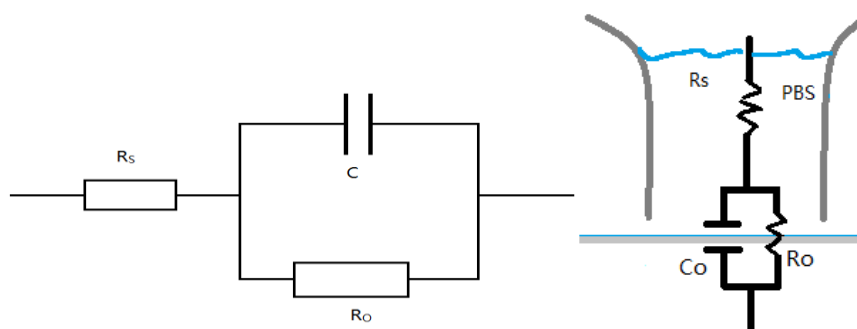


**Figure 3.2** Randle's model

For the external PBS covered condition, a crevice impedance model was utilized,

as shown below. This model, first described by Swaminathan and Gilbert, captures the

effects of both the internal (to the pipette) behavior as well as the contribution of the

external electrode surface. The crevice resistance (Rcr) describes the resistive solution

effects of a tight (or not) junction between the internal pipette solution and the

external solution. This parameter approached zero as the pipette junction became wide

open, while it would approach infinity (and become the Randles circuit described

above) if Rcr became infinite.
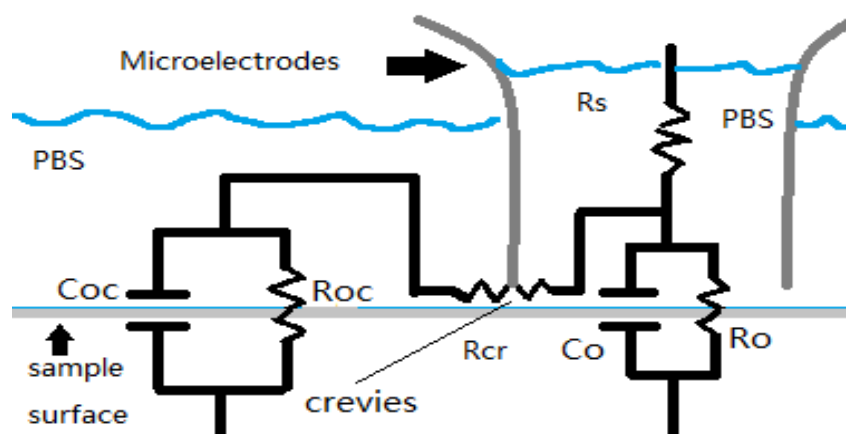


**Figure 3.3** Crevice impedance model and the equivalent circuit

The impedance data are presented in the form of Bode plots and Nyquist plots

and were fitted to the circuit models using a non-linear least squares fitting algorithm

provided with the EIS software. The parameters inside electrolyte resistance ($R_s$),

inside resistance ($R_o$), inside capacitance ($C_o$), outside resistance ($R_{oc}$), outside

capacitance ($C_{oc}$) were determined from the fitting result.

Statistical analysis was performed for every results.

# CHAPTER 4

# RESULTS AND ANALYSIS

## 4.1 Open Circuit Potential

The results from the OCP tests (Fig. 4.1.1) show only small variations in OCP with pipette area for both fluid conditions.
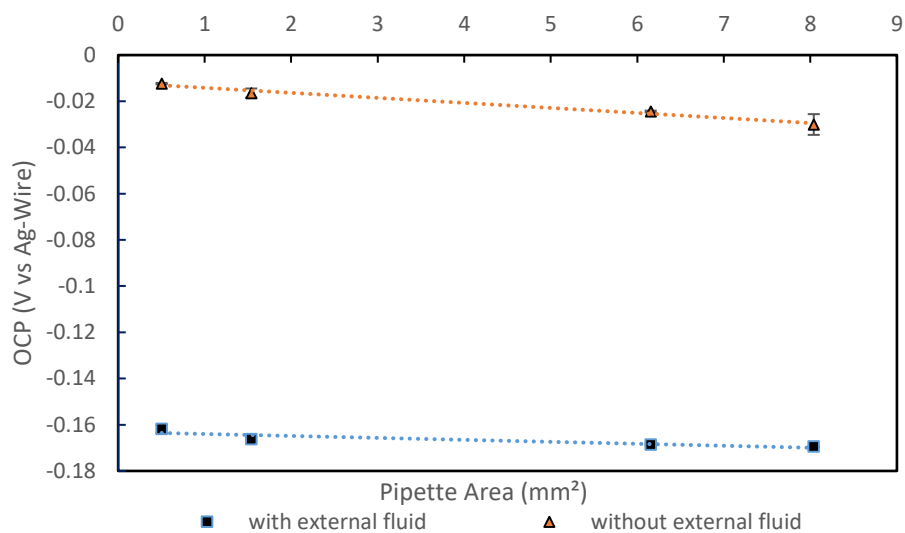


**Figure 4.1.1** CoCrMo alloy OCP measurement within/without external fluid (PBS) condition. Note the significant negative shift in OCP with the presence of external solution present.

The OCP of CoCrMo samples became progressively more negative with increased pipette area. In addition, the OCP of CoCrMo samples was more positive when no external electrolyte was present but with the same pipette area (See Fig. 4.1.1).

All of the p-values for each pair of the results are less than 0.05 (one-way ANOVA). The overall difference is significant (Tukey).
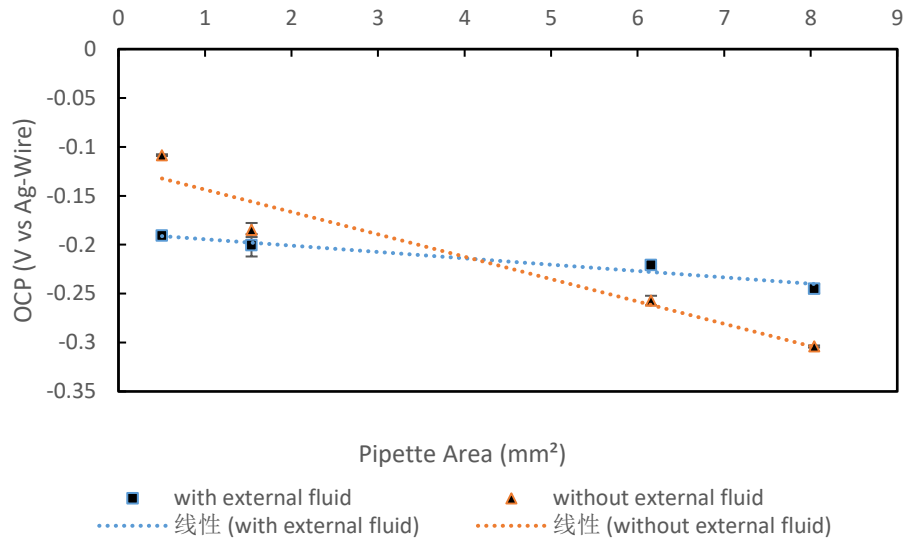
**Figure 4.1.2** Titanium alloy OCP measurement within/without external fluid (PBS) condition

The effect of pipette area on the OCP of Titanium samples (Fig. 4.1.2) shows that the OCP became progressively more negative with increased pipette area in a similar fashion to the CoCrMo results (see Fig. 4.1.2, $P < 0.05$). However, there is not a large shift in OCP between the two solution conditions.

Based on these results, the open circuit potential of CoCrMo alloy and Titanium samples both shift to more negative potentials with increased pipette area with no external solution present.　With external solution, there was less variability in OCP and less of a decrease in OCP with increased pipette area. Additionally, the OCP of CoCrMo sample is more positive in no external electrolyte present condition compared with PBS covered condition on same sample exposing area.

## 4.2 Potentiodynamic Polarization Test

**CoCrMo sample:**
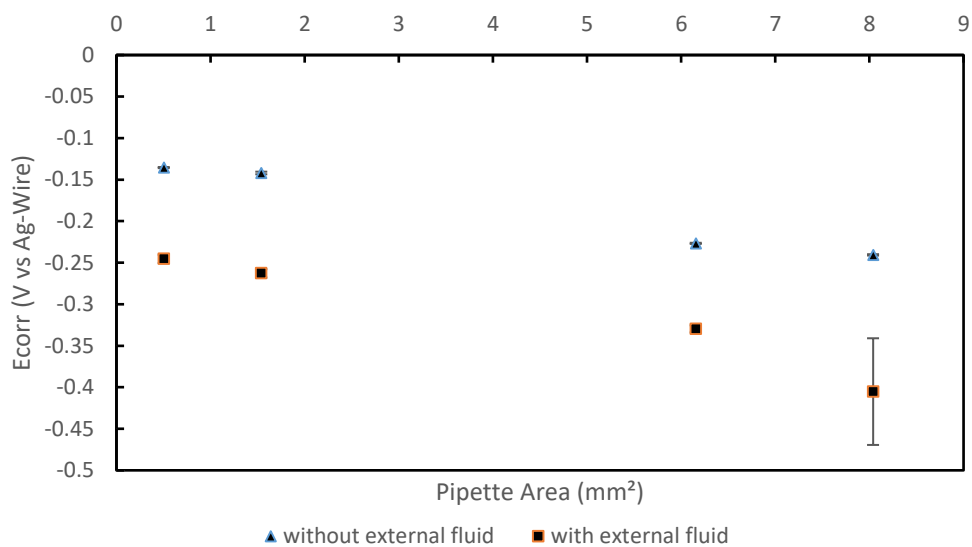


**Figure 4.2.1** $E_{corr}$ of CoCrMo sample within/without external fluid (PBS) condition

The corrosion potential, $E_{corr}$, obtained from the point on the polarization curve where the current changes from cathodic to anodic for CoCrMo became more negative with increased exposed area (See Fig. 4.2.1). Additionally, $E_{corr}$ of CoCrMo sample is shifted to more positive potential in the no-external-electrolyte condition compared with PBS covered condition ($P < 0.05$, See Fig. 4.2.1). This is consistent with the OCP observations shown above.
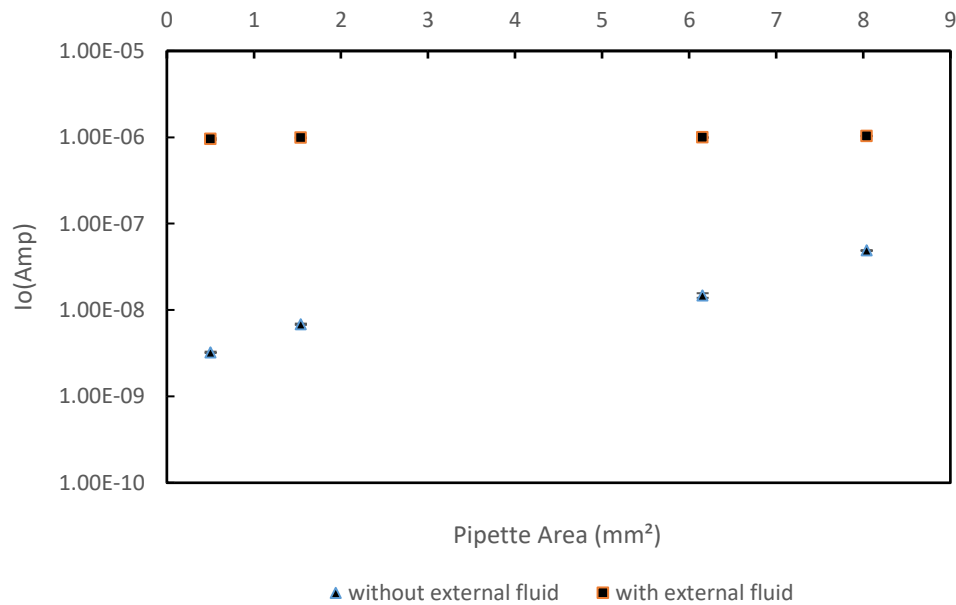
**Figure 4.2.2** $I_{corr}$ of CoCrMo sample within/without external fluid (PBS) condition.

The corrosion current (in Amps) obtained from the polarization plots is plotted against pipette area for both fluid conditions in Fig. 4.2.2. Since the potentiostat was measuring the current density as $Amp/cm^2$, the filter was set as 1 $cm^2$ to get the actual current value to show its variation with electrode area. The corrosion current of CoCrMo increased with exposed area for the no-external solution condition and was approximately constant when external solution was present(See Fig. 4.2.2).    This indicates that the area affects the corrosion current (resulting in a constant current density) and that when the external solution is present, the corrosion currents are generated from the entire surface and not just from the pipette area electrode region. In addition, since the total electrode area was about 100 $mm^2$, the corrosion current is about 100 times the no-external-solution condition, as expected.
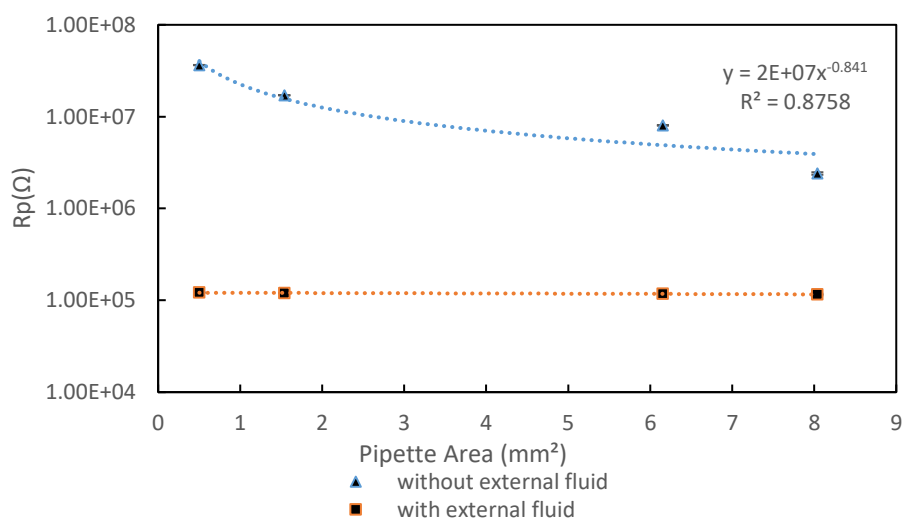
**Figure 4.2.3** Polarization resistance of CoCrMo sample within/without external fluid
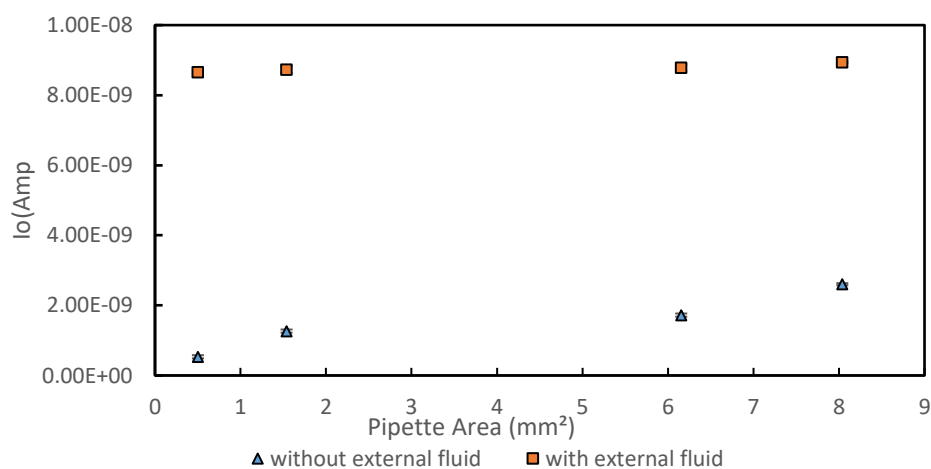
(PBS) condition

The polarization resistance measured from the polarization plot results of

CoCrMo decreased with increased pipette area for the no-external solution case and

varied as 1/A as expected (See Fig. 4.2.3). When external solution was present, Rp did

not vary significantly again indicating that the total electrode area immersed in

contributing to the signal.

**Titanium sample:**
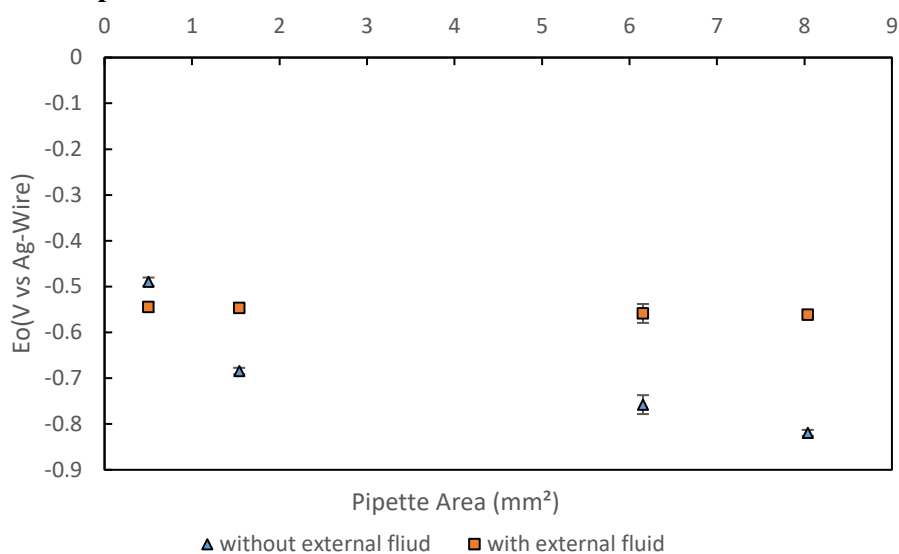


**Figure 4.2.4** $E_{corr}$ of Titanium sample within/without external fluid (PBS) condition

The corrosion potential, Ecorr, of Titanium obtained from the polarization plots, in the no-electrolyte-covered condition became more negative with increased exposed area, while the corrosion potential of Titanium sample in PBS covered condition didn't change much (See Fig. 4.2.4).    It is unclear why these variations in potential are occurring in the no-external-solution condition.



**Figure 4.2.5** Corrosion current of Titanium sample within/without external fluid

(PBS) condition

35

The corrosion current measured from the polarization plots of Ti show a linear increase with area, as expected since the current density should be constant with electrode area, while the corrosion current for the external solution condition did not change significantly with pipette area (see Fig. 4.2.5).
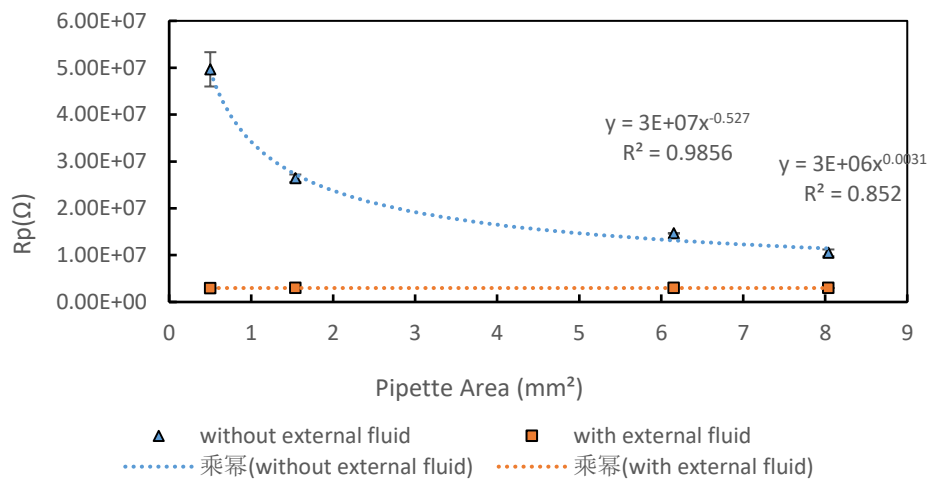


**Figure 4.2.6** Polarization resistance of Titanium sample in the no-electrolyte-covered condition.

The polarization resistance of Titanium, measured from the polarization plots, exhibited an area dependence in the no-electrolyte-covered condition (decreasing with exposed area), while the polarization resistance of Titanium sample in PBS covered condition did not change significantly with increasing exposed area (See Fig. 4.2.6).

## 4.3 Electrochemical Impedance Spectroscope

The EIS response of this system was highly dependent on whether there was external solution present or not.   When so external solution is present, then a CPE-modified Randle's circuit was used to analyze the behavior.   However, when external solution was present, then an alternative crevice-like model, proposed by Gilbert and Swaminathan was utilized.

### 4.3.1   No electrolyte covered condition

In no electrolyte covered condition, the equivalent circuit is shown below:
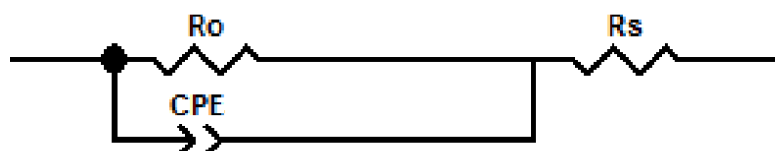


**Figure 4.3.1.1** Randle's circuit CPE model

To closely fit in the data, a constant phase element was introduced to improve the equivalent circuit model.

The impedance $\dfrac{1}{Z} = \dfrac{1}{Rp} + j\omega C$,

Now can be altered into $\dfrac{1}{Z} = \dfrac{1}{Rp} + \text{CPE-T} \,(j\omega)^{\text{CPE-P}}$

Where $\omega$ is frequency, CPE-T is a constant that reflects the capacitance-like character of the surface, and CPE-P is a the exponent which varies between 0 and 1.

The element will behave more like an ideal capacitor when the value is close to 1 and more like a resistor when close to zero.

The typical Nyquist and Bode plot of the impedance response for CoCrMo using different pipette areas are shown in Figs. 4.3.1.2 and 4.3.1.3. It is clear from these results that pipette area systematically decreases the resistive values of the Randle's circuit and alters the phase angle (and capacitive) character as well. Smaller areas result in larger R's. Again, it should be noted that the resistive and capacitive values are not normalized by area but are extrinsic parameters dependent on electrode area.

**CoCrMo**
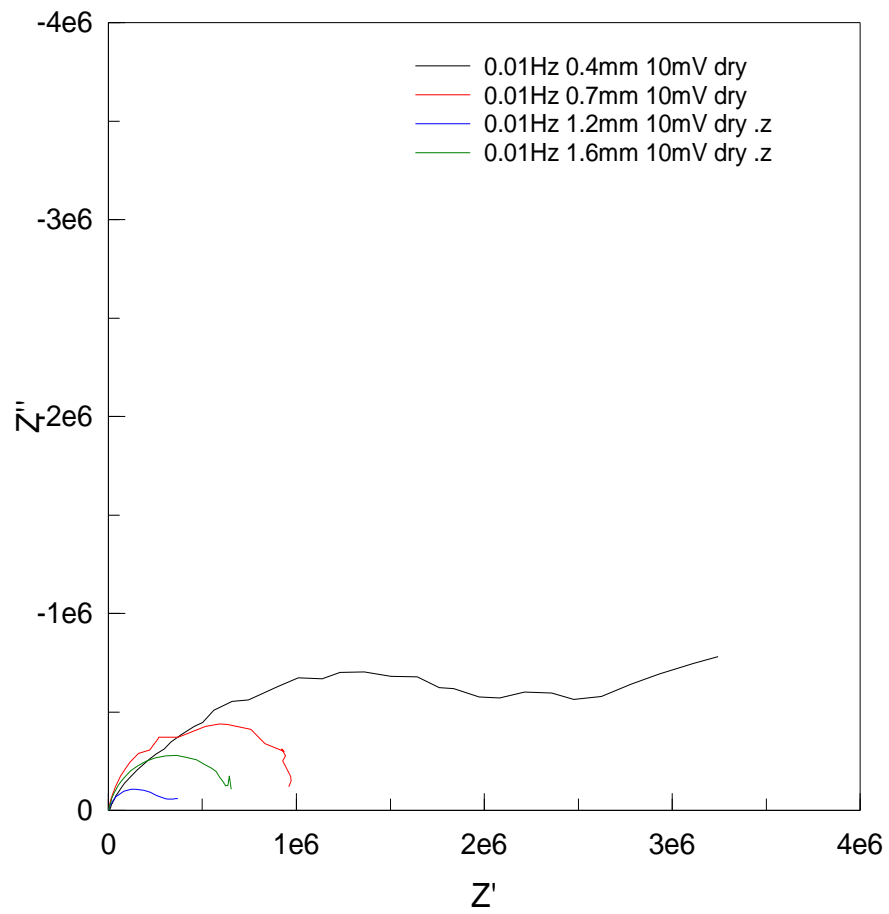


**Figure 4.3.1.2** Nyquist Plot of CoCrMo sample in no electrolyte covered condition
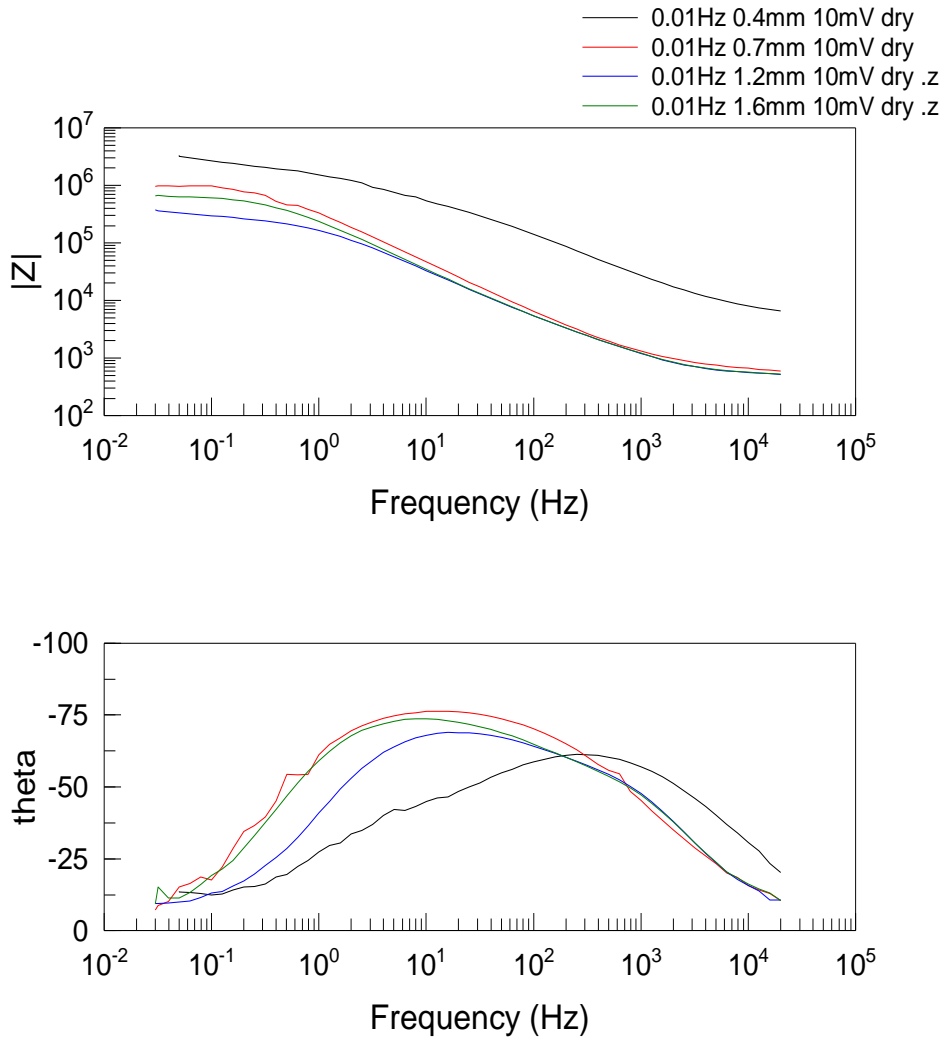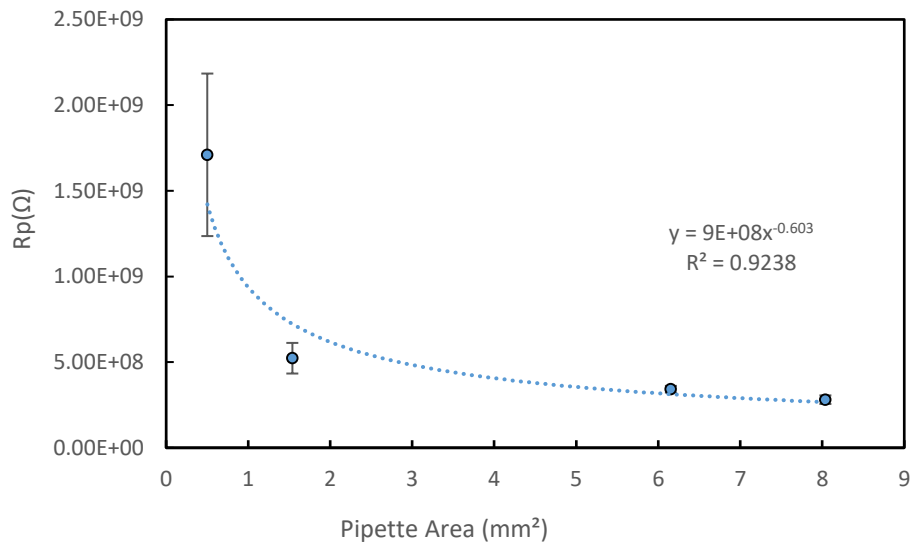
**Figure 4.3.1.3** Bode Plot of CoCrMo sample in no electrolyte covered condition

**Fitting results:**
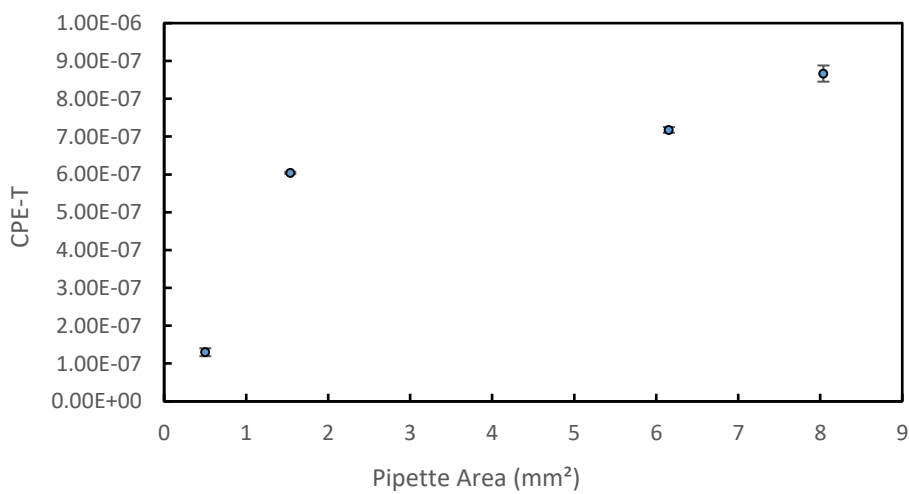


**Figure 4.3.1.4** CoCrMo sample CPE-T in no electrolyte condition.

The CPE-T values increase with increasing exposed area (See Fig. 4.3.1.4), as is expected. However, the values for the 2 mm case appear to be outliers to the predicted linear increase with area.



**Figure 4.3.1.5** CoCrMo sample $R_p$ in no electrolyte condition.

The $R_p$ values measured using the CPE-modified Randle's circuit decreased with the increasing area (See Fig. 4.3.1.5) in an approximate 1/A like dependence.
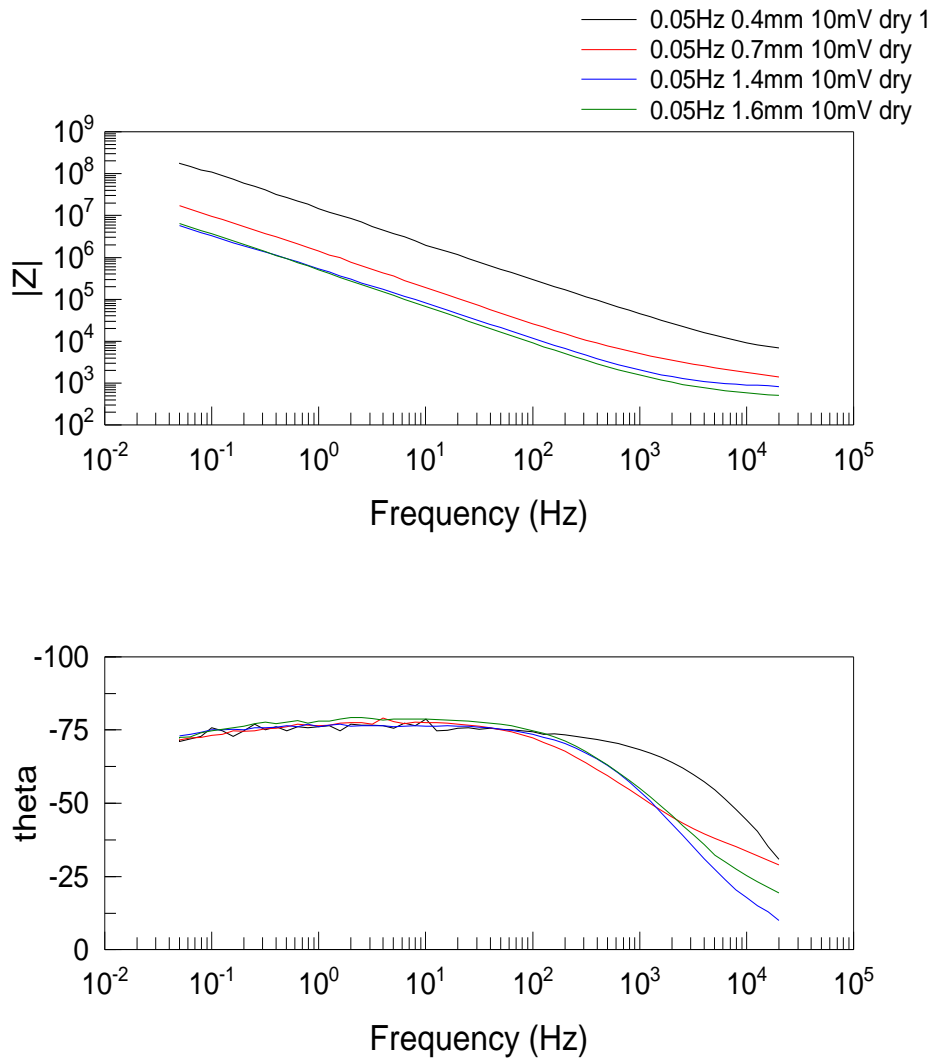
**Titanium**

The results for the titanium electrodes show some similarities to the CoCrMo results in terms of the effects of area and exposed solution conditions. The Nyquist plot (Fig. 4.3.1.6) and Bode plots (Fig. 4.3.1.7) reflect the behavior of the no-external solution tests and increased pipette area.
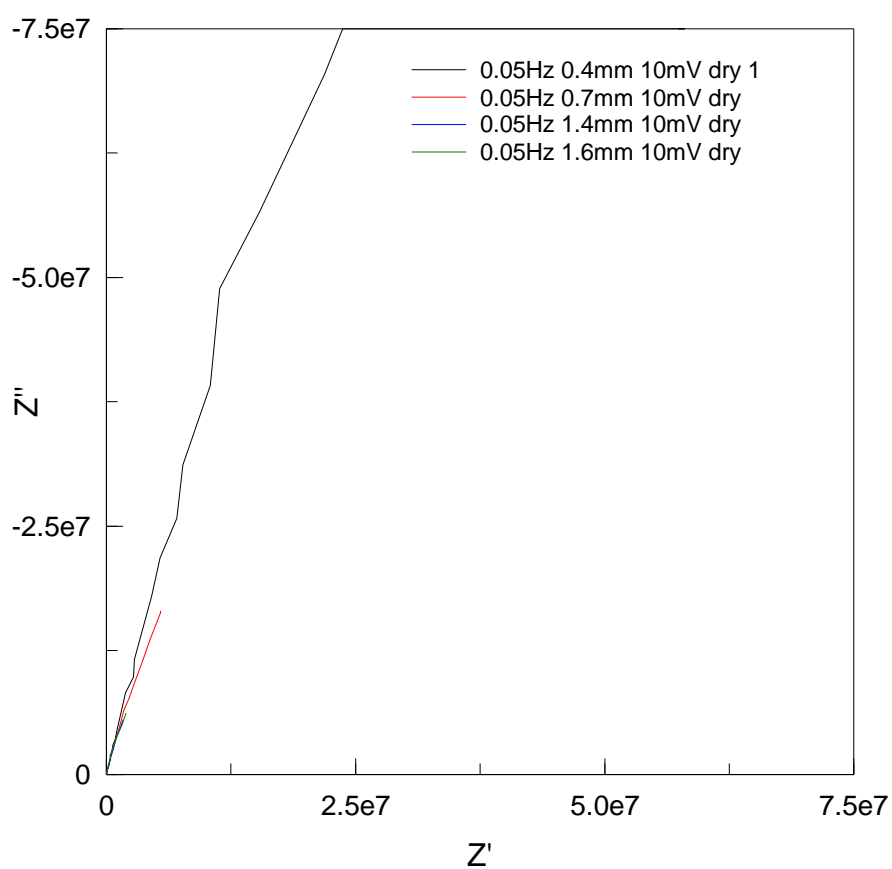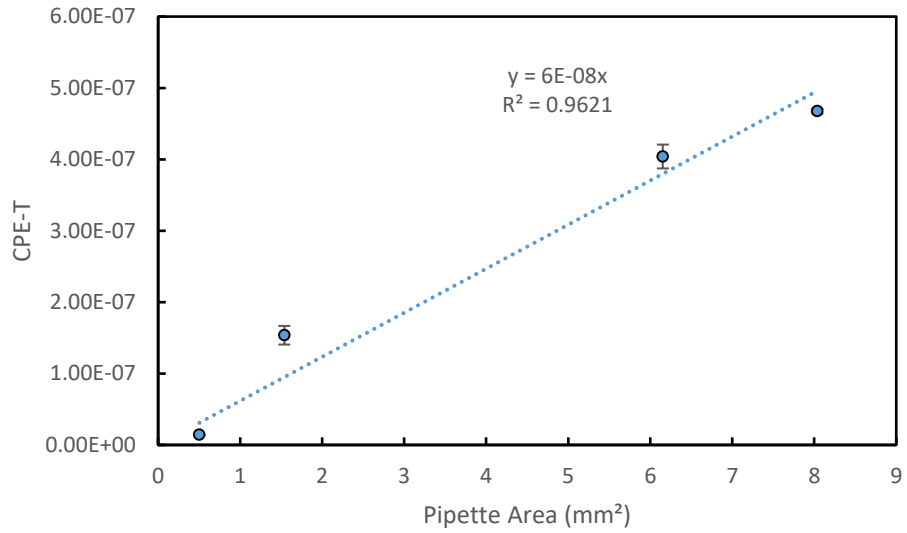


**Figure 4.3.1.6** Nyquist Plot of Titanium sample in no electrolyte covered condition

**Figure 4.3.1.7** Bode Plot of Titanium sample in no electrolyte covered condition

In all instances shown, the low-frequency response (for both Z and phase angle) have not identified the plateau region at 0.01 Hz which makes fitting the Rp for the circuit more challenging.

**Figure 4.3.1.8** Titanium sample CPE-T in no electrolyte condition

The CPE-T (capacitance-like) value is increased with increasing exposed area (See Fig. 4.3.1.8).
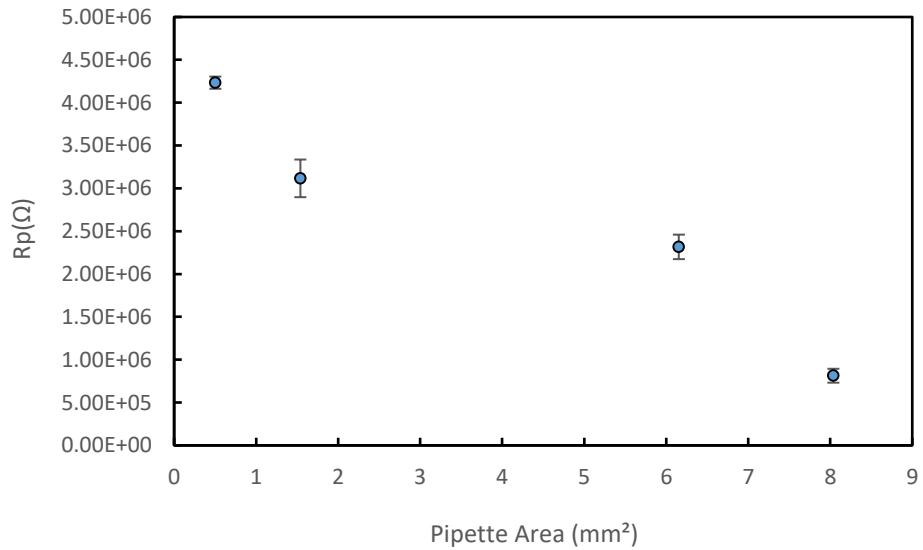


**Figure 4.3.1.9** Titanium sample $R_p$ in no electrolyte condition

The Rp again decreased with increasing exposed area (See Fig. 4.3.1.9).

## 4.3.2 In PBS Covered Condition

When external solution is present, then the behavior of the electrode system is modified and a modified the equivalent circuit is required and is shown below:
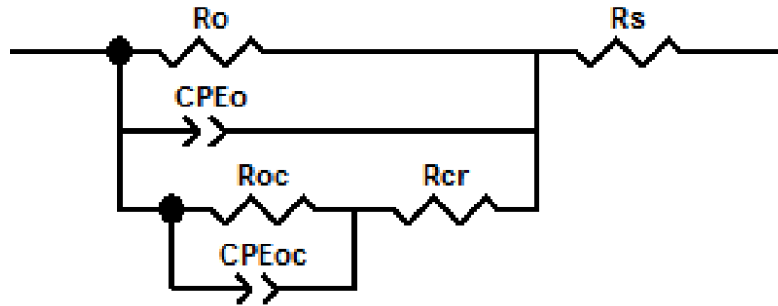


**Figure 4.3.2.1** Gilbert Crevice Impedance CPE model

To closely fit in the data, a Gilbert crevice impedance model was introduced and slightly altered by inclusion of CPE elements instead of ideal capacitors, to improve the equivalent circuit model. The impedance in this condition can be calculated by following equations:

$$\tau_{oc} = R_{oc} \cdot CPEoc - T \cdot (j\omega)^{CPEoc - P}$$

$$\tau_{o} = R_{o} \cdot CPEo - T \cdot (j\omega)^{CPEo - P}$$

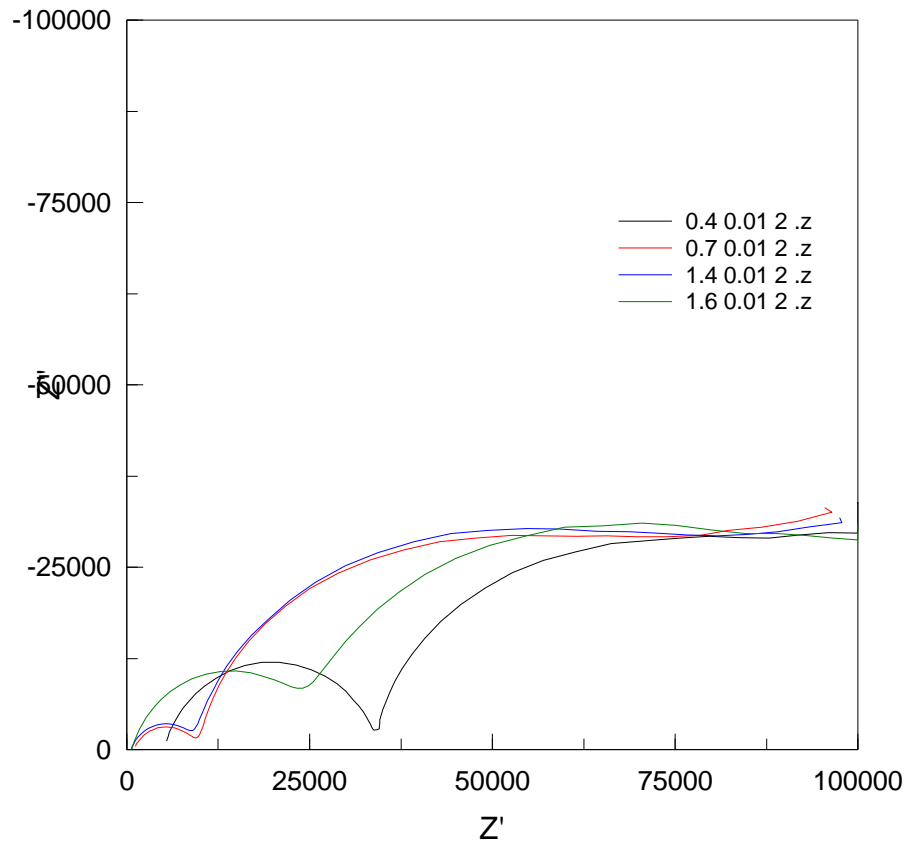$$Z'_{oc} = R_{cr} + \frac{R_{oc}}{1 + (\omega\tau_{oc})^2}$$

Where

$$Z''_{oc} = -iR_{oc} \frac{\omega\tau_{oc}}{1 + (\omega\tau_{oc})^2}$$

$$a = R_{o} + Z'_{oc} - \omega\tau_{o} Z''_{oc}$$

$$b = Z''_{oc} + \omega\tau_{o} Z'_{oc}$$

$$Z_{||} = \frac{R_{o}}{a^2 + b^2} \left[ \left( Z'_{oc} a + Z''_{oc} b \right) + i \left( aZ''_{oc} - bZ'_{oc} \right) \right]$$
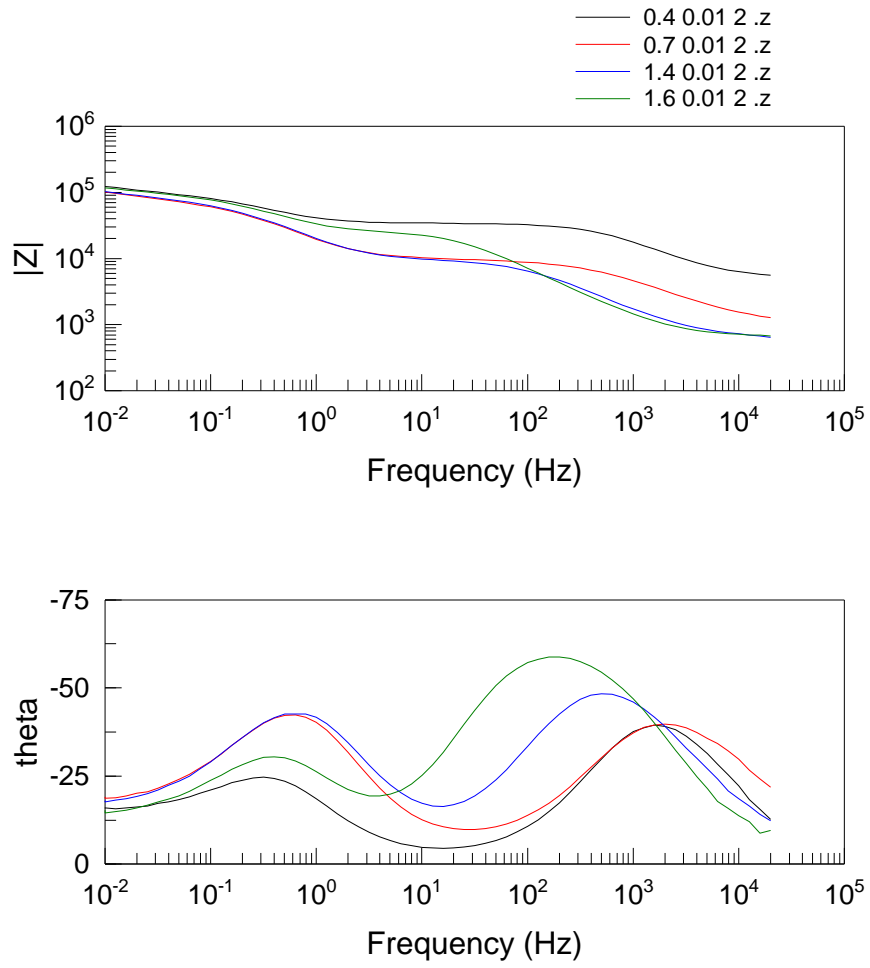
**CoCrMo sample:**



**Figure 4.3.2.2** Nyquisit Plot of CoCrMo sample in PBS covered condition.

The typical Nyquist plot of the CoCrMo sample when external solution is present

for different pipette areas is shown in Fig. 4.3.2.2. A characteristic double circular

response is seen where the first circle changes its radius with pipette area.

The corresponding Bode plots for these experiments are shown in Fig. 4.3.2.3.

Systematic changes in Z and phase angle with pipette area are demonstrated in these

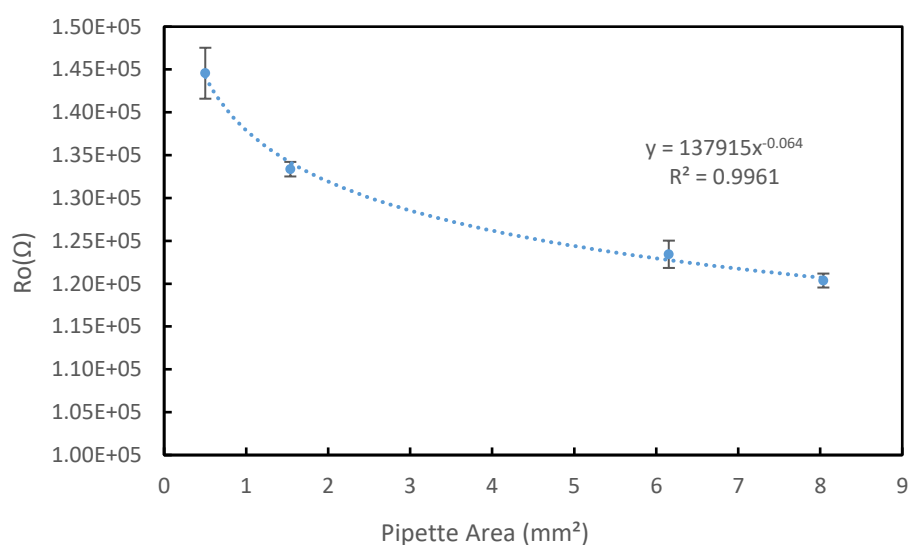plots, particularly at the intermediate and high frequencies.

**Figure 4.3.2.3** Bode Plot of CoCrMo sample in PBS covered condition.

**Fitting results:**

Then CPE-modified crevice model did an excellent job fitting the resultant data. From the fit of this model to the data, various parameters associated with the model can be evaluated for the effects of pipette area.
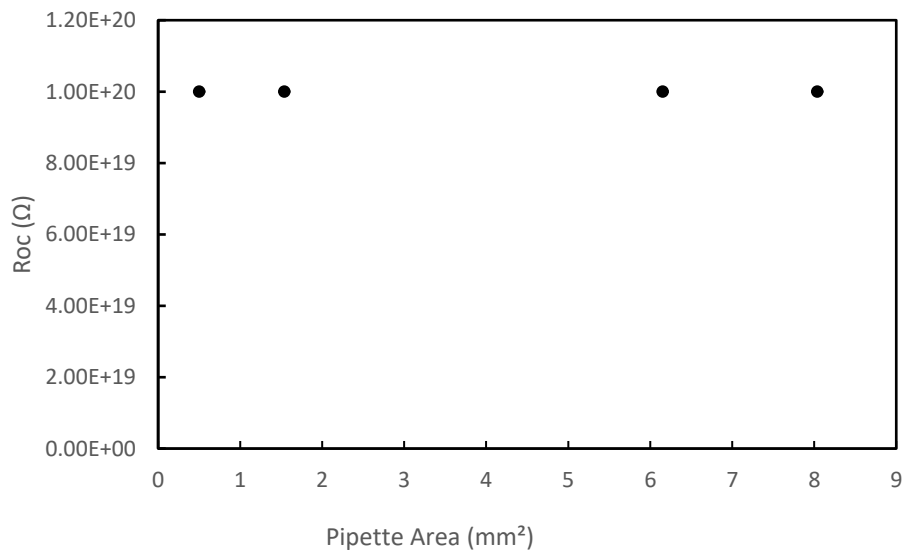


**Figure 4.3.2.4** Ro of CoCrMo sample in PBS covered condition

It can be seen, for example, that the values of Ro (the internal pipette surface resistance) decreased with increased exposed area (See Fig. 4.3.2.4), even though the external solution was present. The area dependence of Rp was not a large as that obtained from the polarization data and is distinct from it.
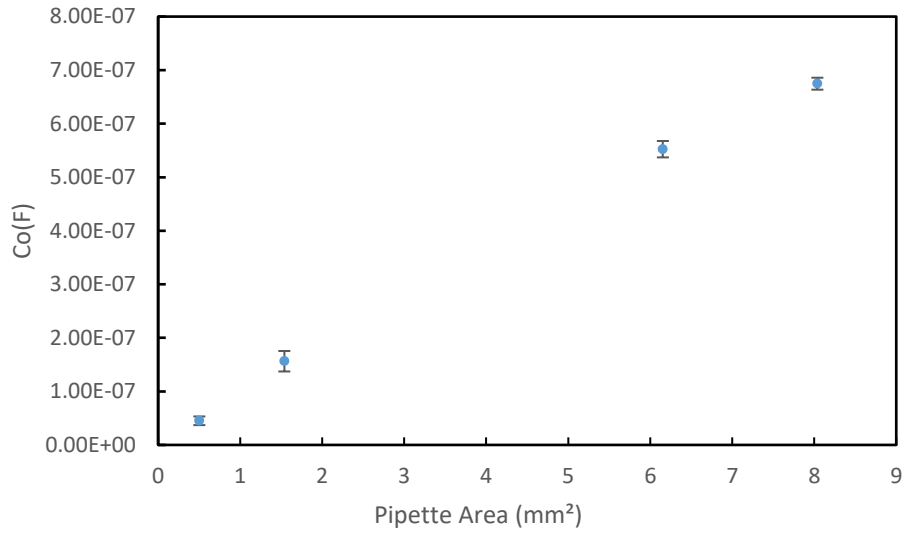
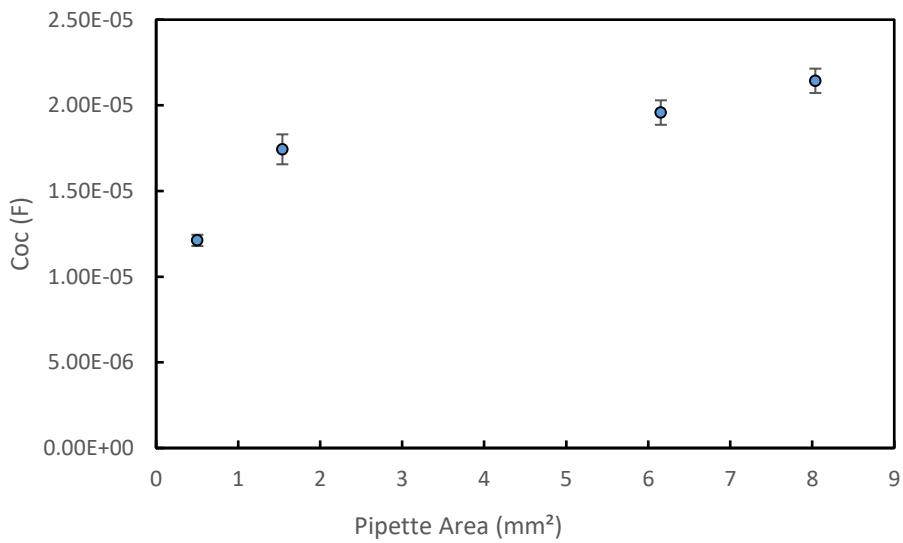**Figure 4.3.2.5** Co of CoCrMo sample in PBS covered condition

The values of Co (the internal CPE element) increased with increased pipette area (See Fig. 4.3.2.5).    This is, again, the expected effect of increasing pipette area.



**Figure 4.3.2.6** Roc of CoCrMo sample in PBS covered condition

The values of the external electrode area resistance, Roc, are not significantly affected by changes in pipette area, and in this case, the non-linear curve fitting could not determine this value to be different from the upper limit resistance in the system (See Fig. 4.3.2.6).



**Figure 4.3.2.7** Coc of CoCrMo sample in PBS covered condition

The values of the external capacitance circuit element, Coc, increased with increased pipette area (See Fig. 4.3.2.7).
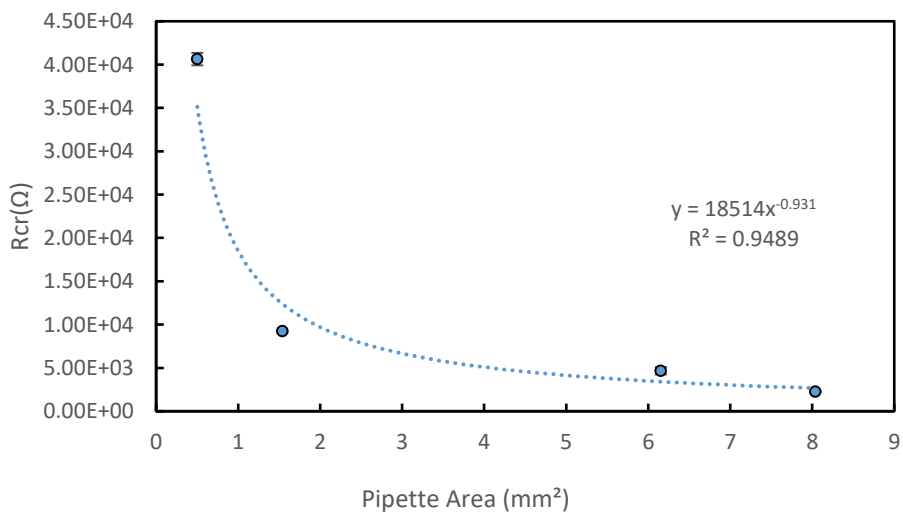


**Figure 4.3.2.8** Rcr of CoCrMo sample in PBS covered condition

The value of the crevice resistance, Rcr, decreased, in a 1/A dependence, with pipette area (See Fig. 4.3.2.8). This parameter is also highly sensitive to the distance of the pipette tip to the electrode surface (as will be shown below). In these tests, the distance was kept relatively constant.

**Titanium sample:**

The behavior of Ti sample in the crevice model conditions are summarized in the Nyquist plot (Fig. 4.3.2.9) and Bode plots (Fig. 4.3.2.10) below. The effects of pipette area are similar to that seen in CoCrMo alloy electrodes and show an effect of pipette area on impedance.
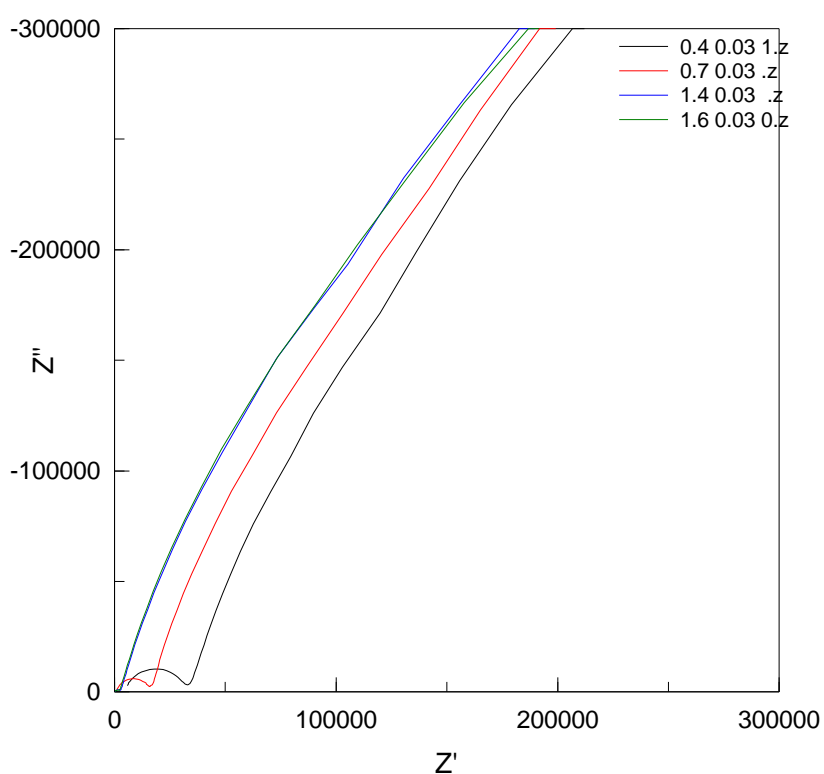


**Figure 4.3.2.9** Nyquisit Plot of Titanium sample in PBS covered condition

The effects of pipette area are most evidence in the Bode plots where the mid-frequency plateau represents the crevice resistance and the changing Rs at high frequencies is a direct reflection of the pipette area.
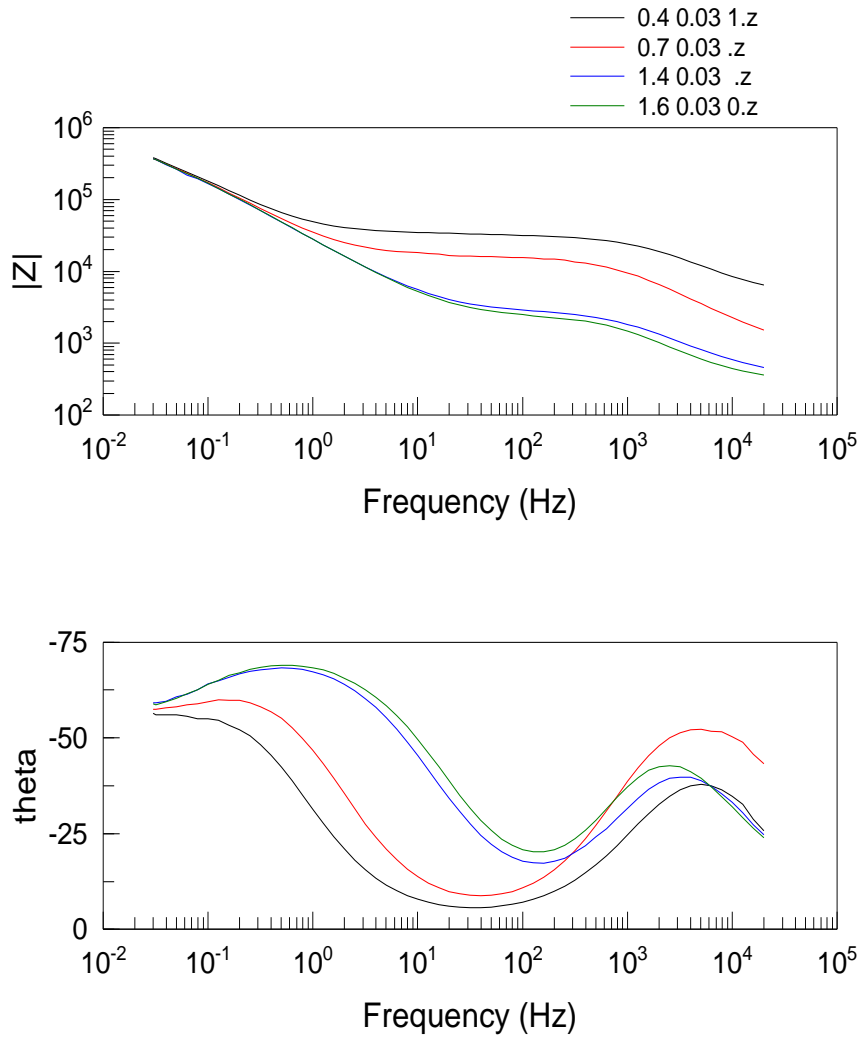
**Figure 4.3.2.10** Bode Plot of Titanium sample in PBS covered condition

**Fitting results:**

The results of fitting of the crevice impedance model to the data are shown

below.
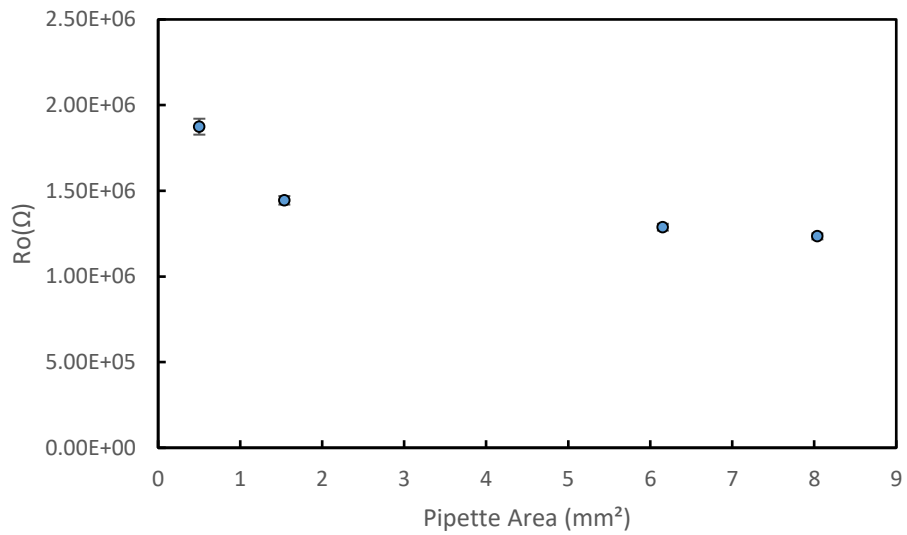


**Figure 4.3.2.11** Ro of Titanium sample in PBS covered condition

The value of the internal surface resistance, Ro, decreased with increased area, as

was seen for CoCrMo electrodes (See Fig. 4.3.2.11).
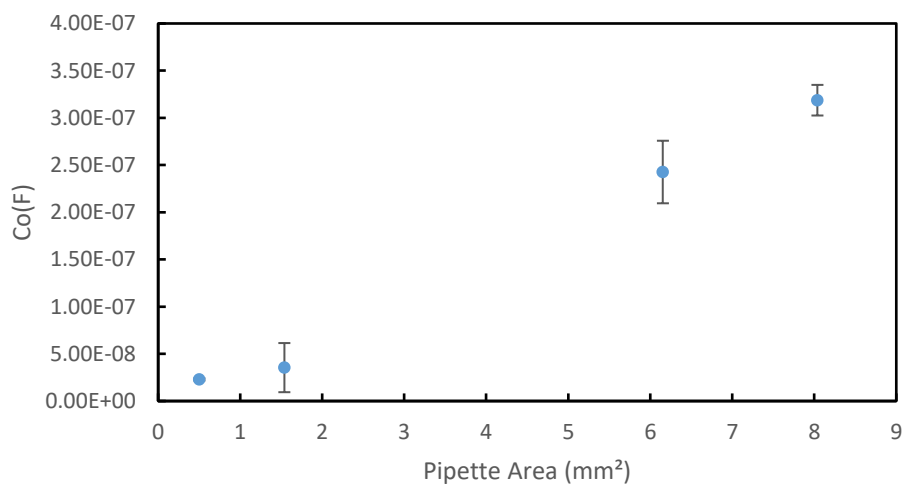


**Figure 4.3.2.12** Co of Titanium sample in PBS covered condition

The value of internal capacitance, Co, increased linearly with pipette area (See

Fig. 4.3.2.12).
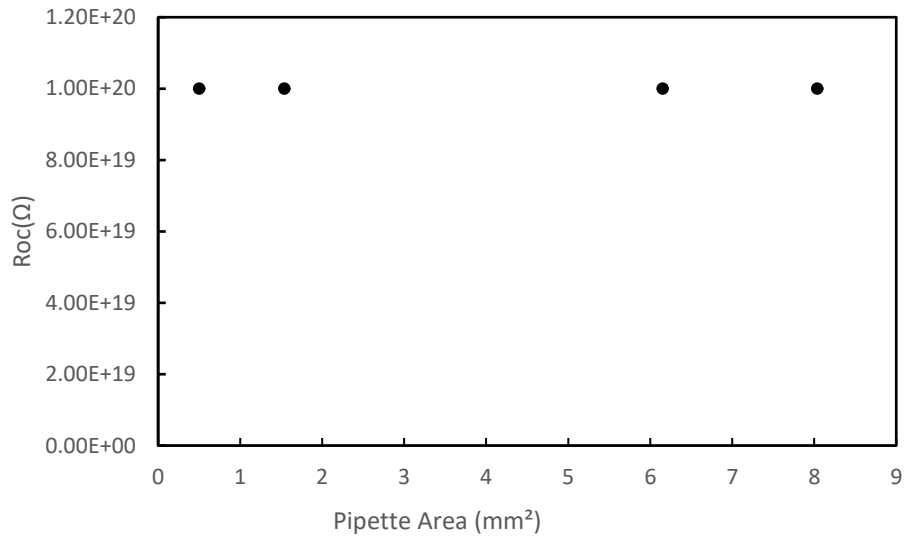


**Figure 4.3.2.13** Roc of Titanium sample in PBS covered condition

The values of the external surface resistance, Roc, were beyond the measurement

range (See Fig. 4.3.2.13).



**Figure 4.3.2.14** Coc of Titanium sample in PBS covered condition

The values of the external capacitance, Coc, were not affected by pipette are since the external electrode area was close to 100 mm$^2$ (See Fig. 4.3.2.14).



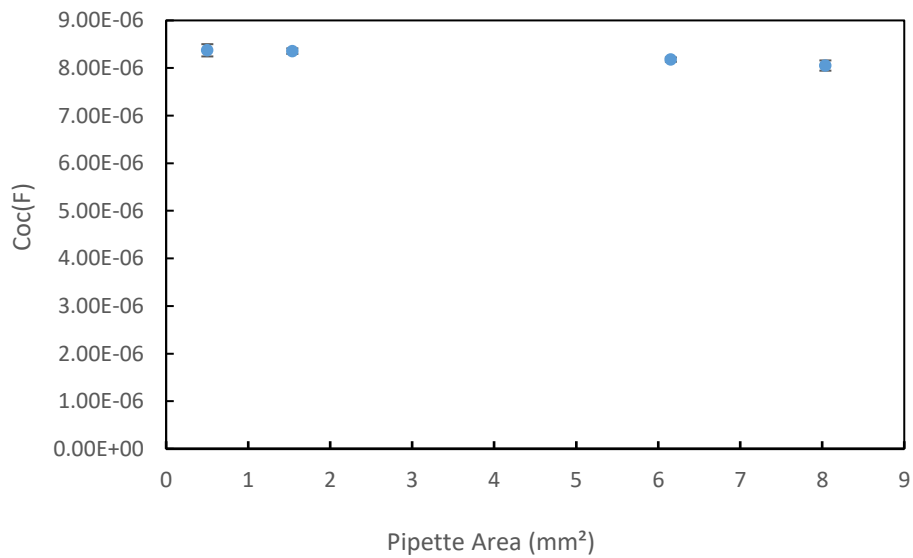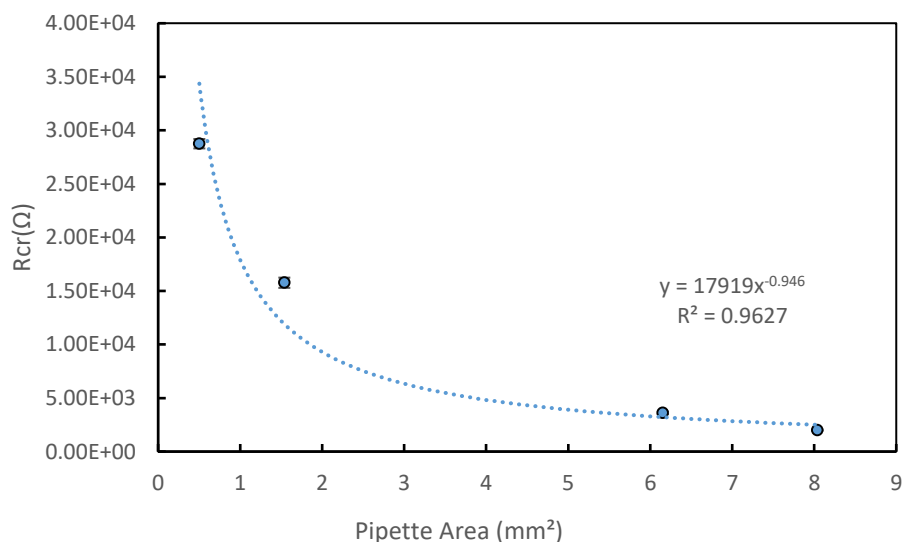The chart shows Rcr($\Omega$) on the y-axis ranging from 0.00E+00 to 4.00E+04 versus Pipette Area (mm²) on the x-axis ranging from 0 to 9, with a fitted curve labeled $y = 17919x^{-0.946}$ and $R^2 = 0.9627$.

**Figure 4.3.2.15** Crevice resistance, Rcr, of Titanium sample in PBS covered condition

The value of Rcr decreased with pipette area, as expected (See Fig. 4.3.2.15). This trend is very similar to that found for the CoCrMo Rcr case.

## 4.4 CoCrMo sample in PBS covered condition versus different height from electrode to sample surface

The effect of the pipette-electrode height on the impedance response when external fluid is present are summarized in this section.   A pipette of fixed area was placed above the electrode and a precision micrometer adjusted the height of the pipette tip to the electrode surface.   The position where the tip made physical contact with the electrode surface was not well controlled but was within the range of distances tested.   Once the pipette made contact, increased

movement of the micrometer simply applied greater contact loads between the

tip and electrode which may have continued to affect the crevice resistance.
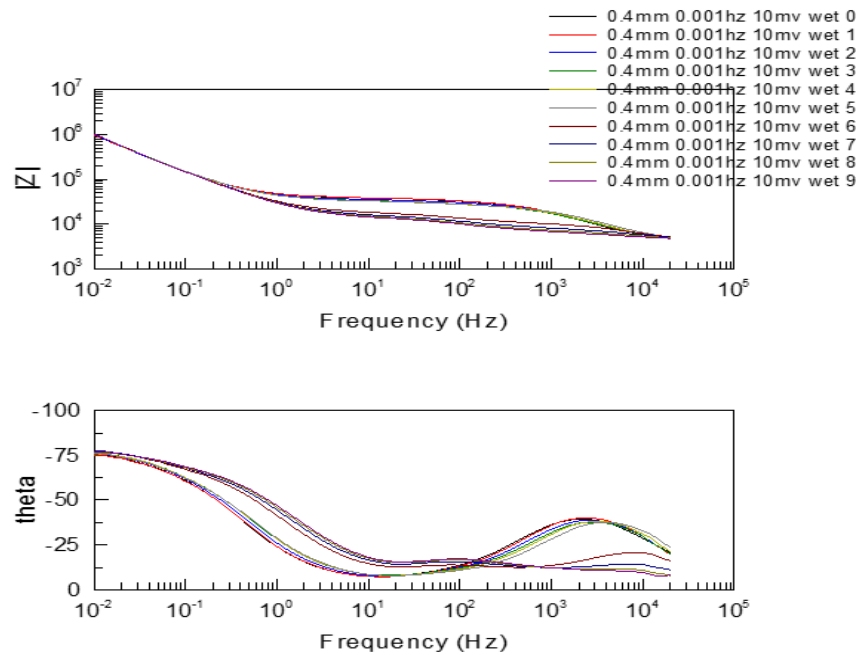


**Figure 4.4.1.1** Bode Plot of CoCrMo sample in PBS condition vs. different height (0.4mm radius electrode )
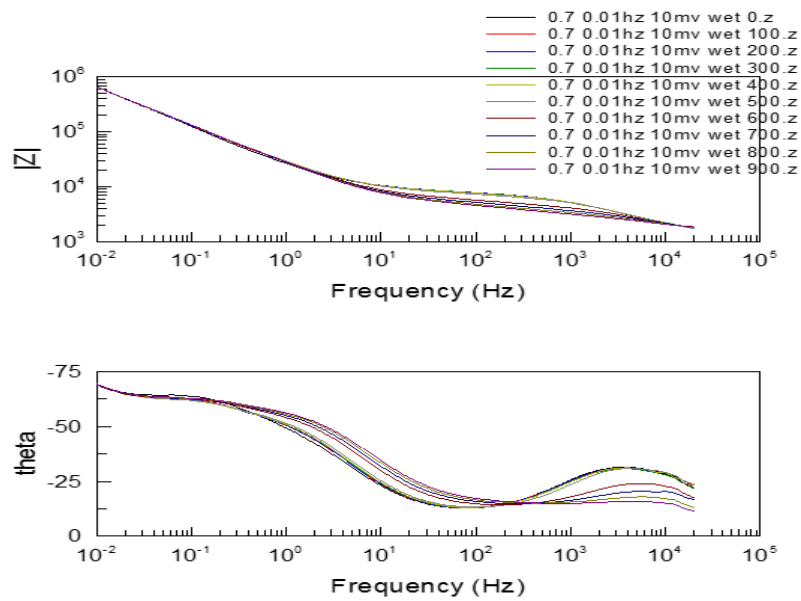


**Figure 4.4.1.2** Bode Plot of CoCrMo sample in PBS condition vs. different height (0.7mm radius electrode )
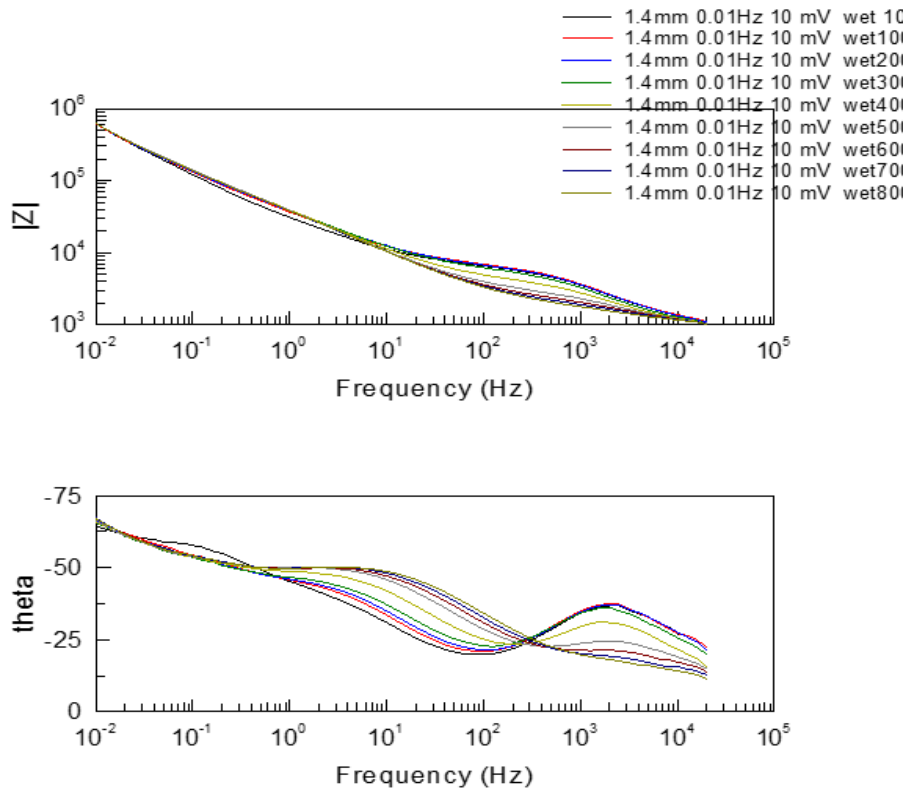
**Figure 4.4.1.3** Bode Plot of CoCrMo sample in PBS condition vs. different height
((1.4mm d radius electrode )
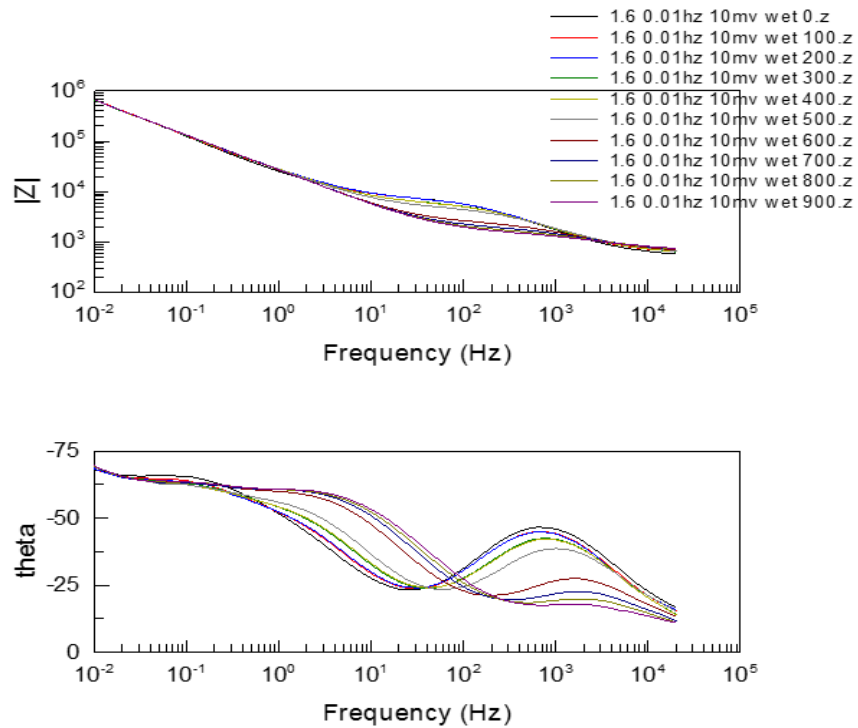


**Figure 4.4.1.4** Bode Plot of CoCrMo sample in PBS condition vs. different height
(1.6mm radius electrode )

The effect of pipette height on the impedance response for the four different pipette areas explored are summarized in Figs. 4.4.1.1 to 4.4.1.4.   In all cases, the response was similar in appearance with the characteristic double bump phase angle response and the plateau of the crevice resistance in the Z vs frequency plots.   There are systematic changes in the plateau resistance (crevice resistance) and the frequencies for the peaks in the phase angle that change with tip-surface distance.

From these plots, the characteristic parameters of the crevice impedance model can be determined and plotted against tip-sample distance. These results are summarized below.

**Fitting results:**

The Rcr variations with tip-electrode distance show a consistent behavior with an increased Rcr with smaller distance (or tighter contact). This can be seen in Figs. 4.4.1.5 through Fig. 4.4.1.9.
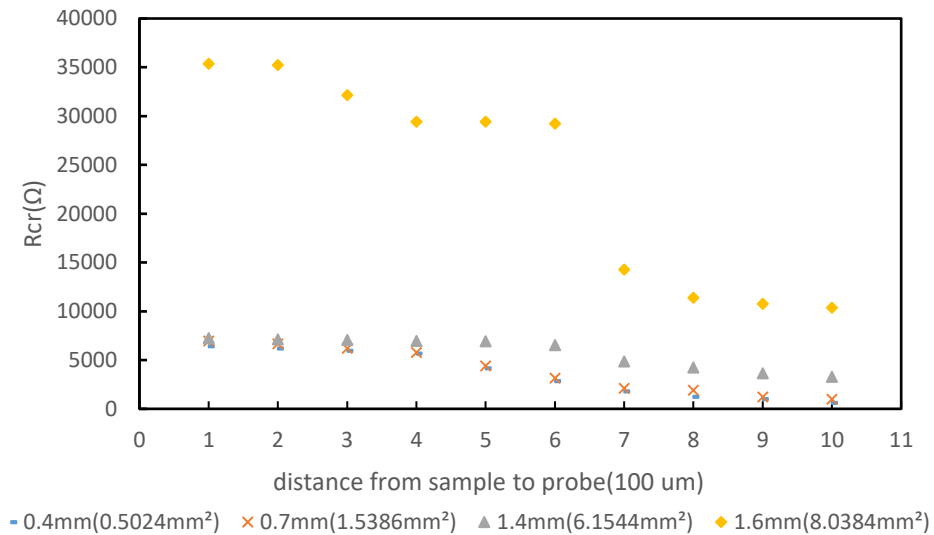


**Figure 4.4.1.5** Rcr value vs distance above CoCr sample surface
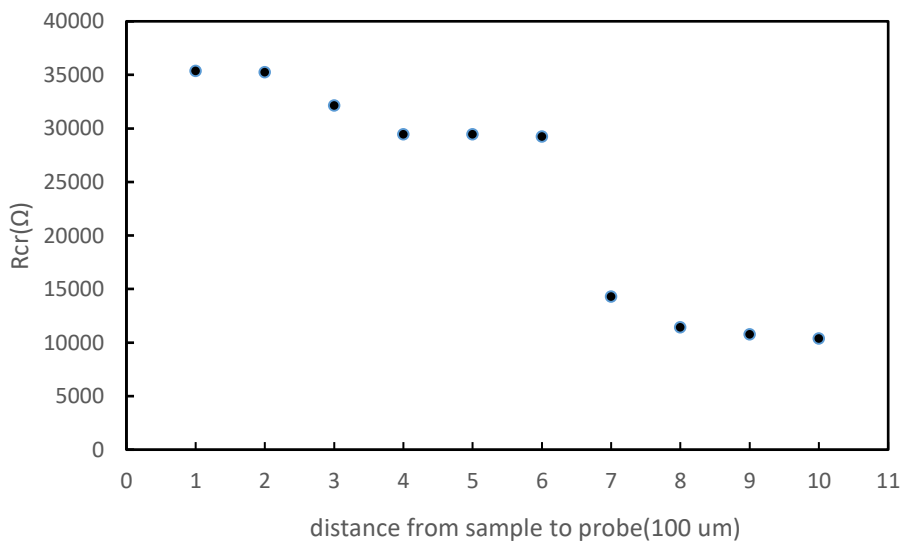


**Figure 4.4.1.6** Rcr value vs distance above CoCr sample surface (0.4 mm radius electrode)
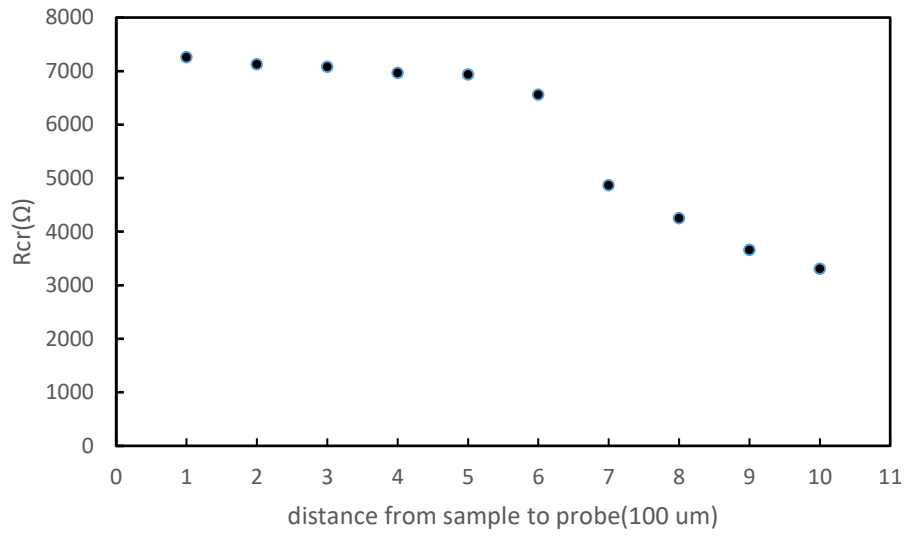
**Figure 4.4.1.7** Rcr value vs distance above CoCr sample surface (0.7 mm radius electrode )
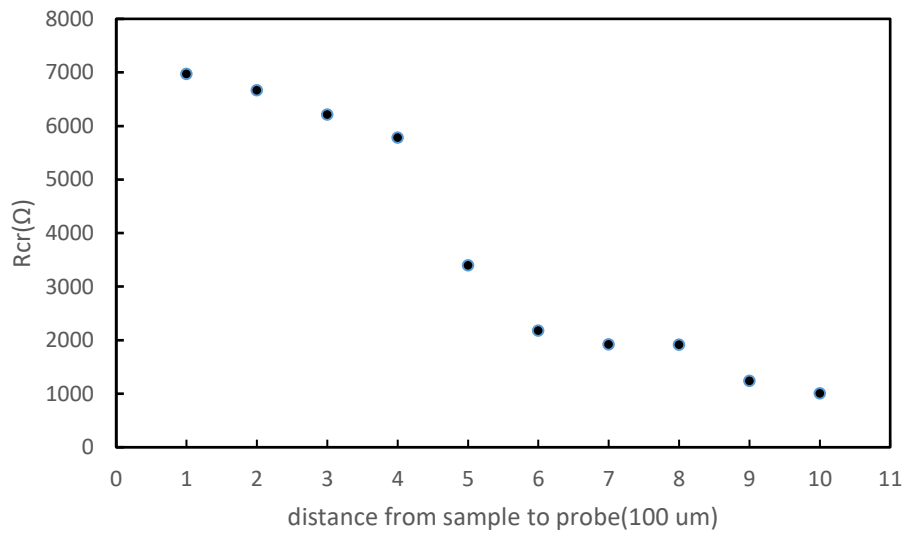


**Figure 4.4.1.8** Rcr value vs distance above CoCr sample surface (1.4 mm radius electrode)

**Figure 4.4.1.9** Rcr value vs distance above CoCr sample surface (1.6 mm radius electrode )

All other parameters of the crevice impedance model did not appear to be affected significantly by the tip-electrode distance changes.

## 4.4.2 Titanium sample in PBS covered condition versus different height from electrode to sample surface

As with the CoCrMo electrodes, when Ti electrodes are tested, similar results are observed. That is, the high frequency and low frequency portions of the impedance plots remain unchanged, however, the crevice resistance (or plateau) of the impedance plot is systematically affected by tip-electrode distance.
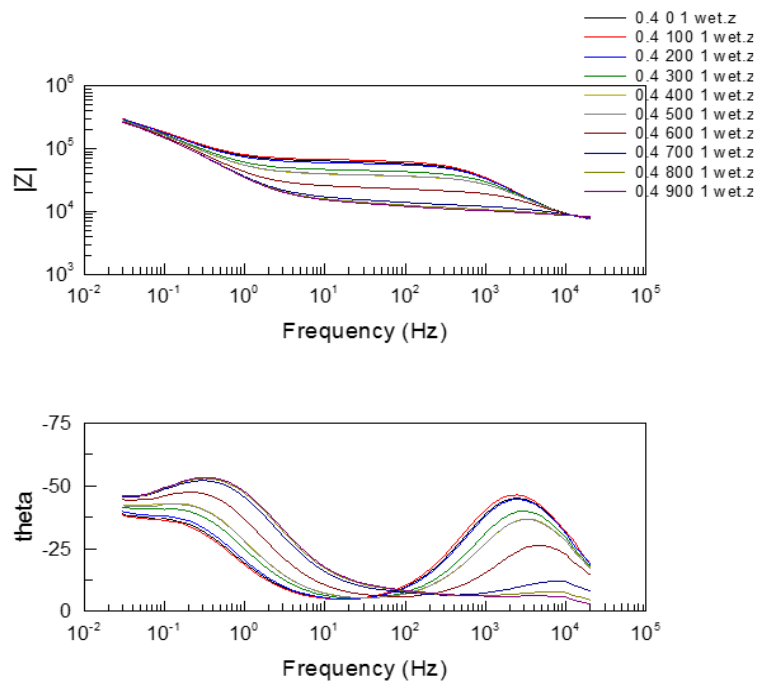


**Figure 4.4.2.1** Bode Plot of Titaium sample in PBS condition vs. different height (0.4mm radius electrode )
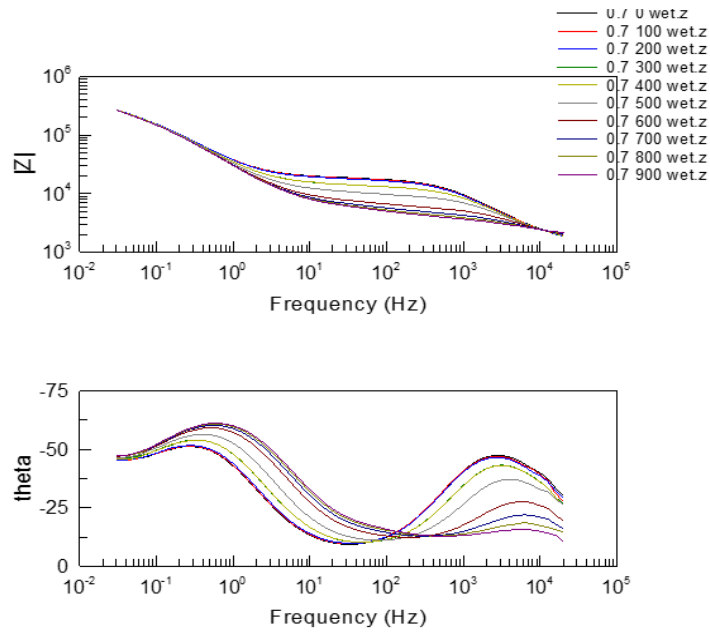
**Figure 4.4.2.2** Bode Plot of Titaium sample in PBS condition vs. different height (0.7mm radius electrode )
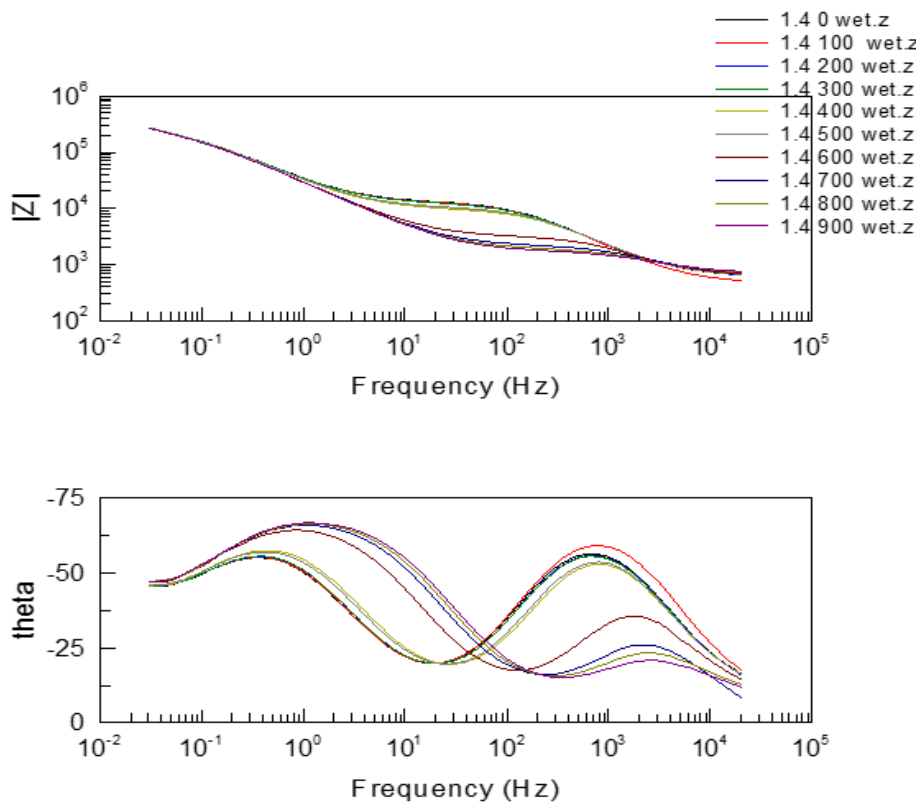


**Figure 4.4.2.3** Bode Plot of Titaium sample in PBS condition vs. different height (1.4mm radius electrode )
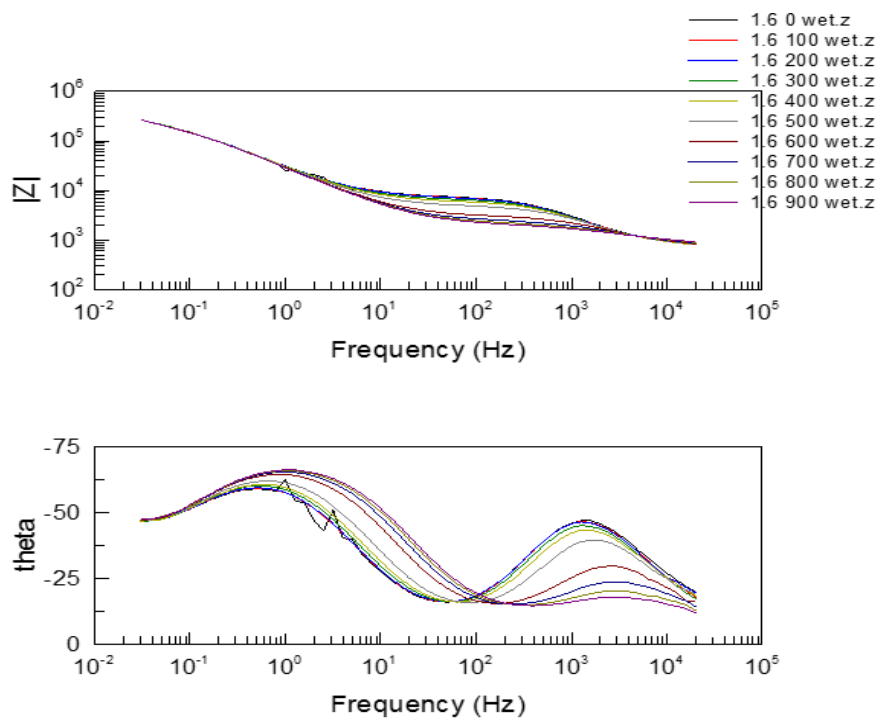
**Figure 4.4.2.4** Bode Plot of Titaium sample in PBS condition vs. different height (1.6 mm radius electrode )

The Rcr and the 2$^{nd}$ plateau of the phase angel vs frequency shifted down with increasing distance between sample surface and electrode probe. (See Fig. 4.4.2.1~4.4.2.4)

**Fitting results:**

The fitting of these results again show that the Rcr is the principal variable affected by

the distance.
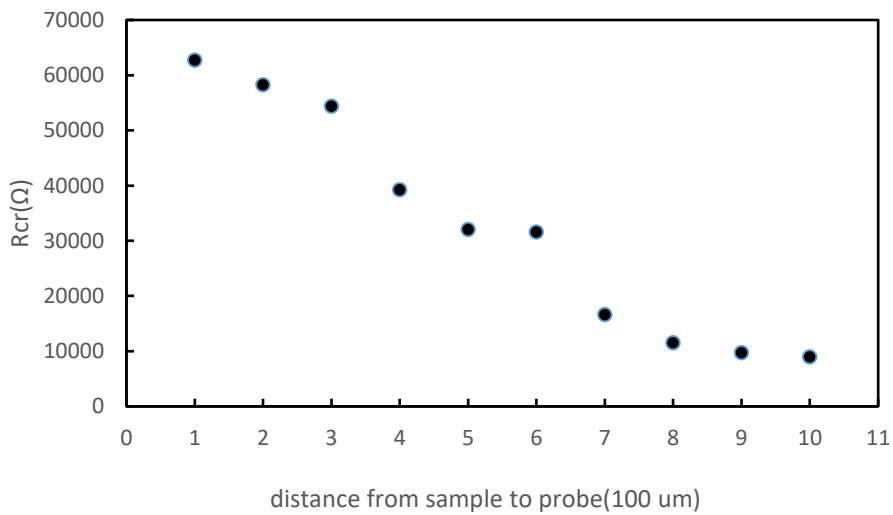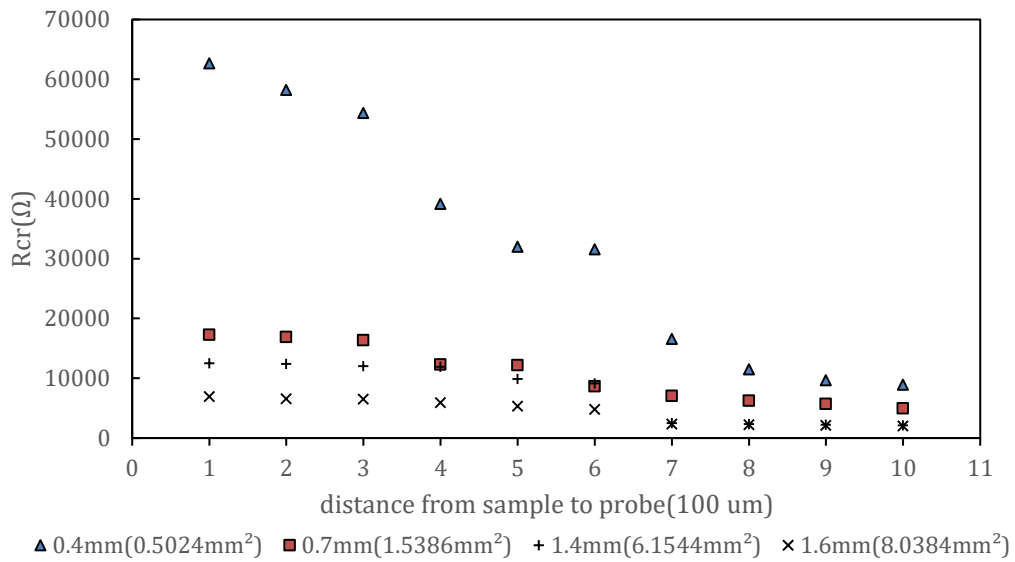


**Figure 4.4.2.6** Rcr value vs distance above Titanium sample surface (0.4 mm radius
electrode )
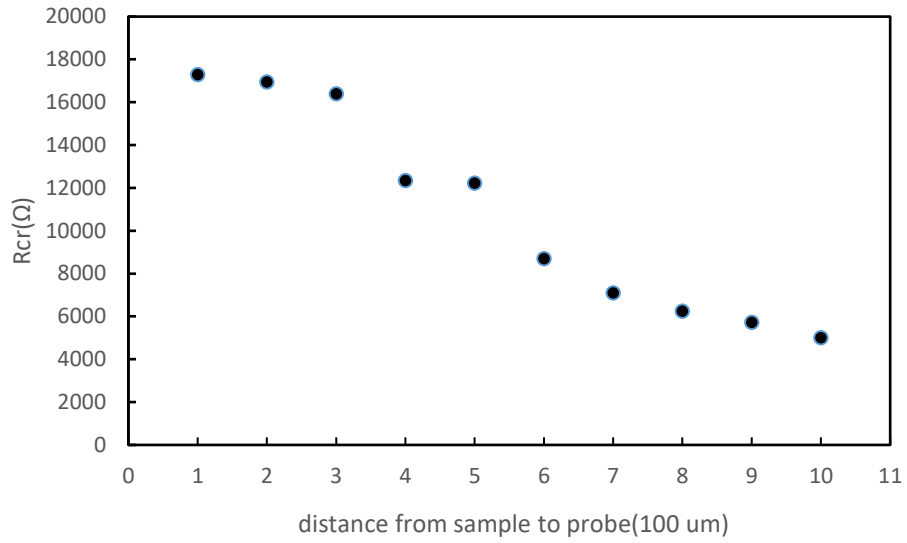
**Figure 4.4.2.7** Rcr value vs distance above Titanium sample surface (0.7 mm radius electrode )
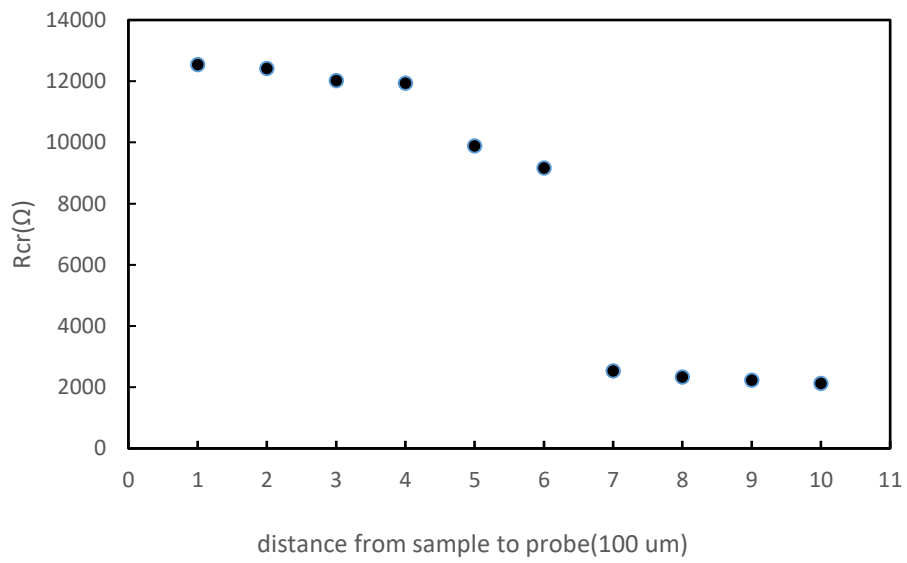


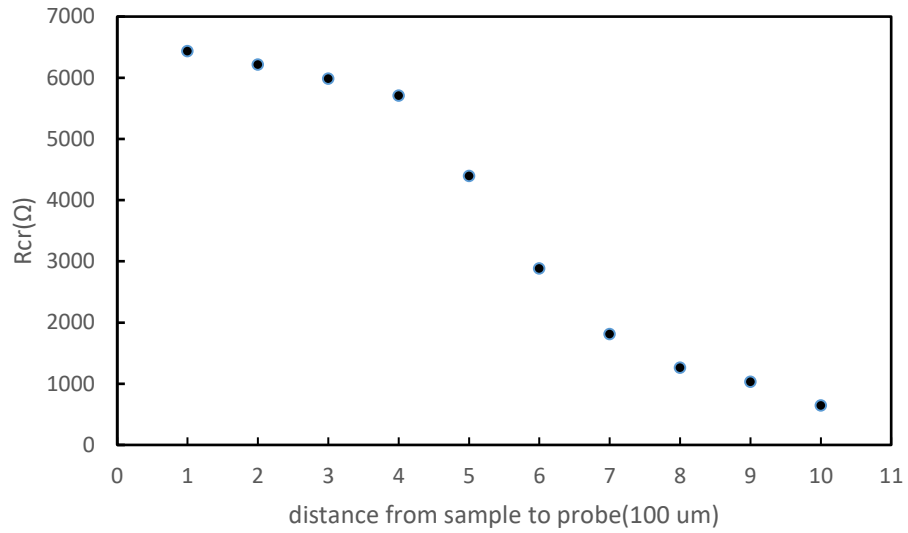**Figure 4.4.2.8** Rcr value vs distance above Titanium sample surface (1.4 mm radius electrode )
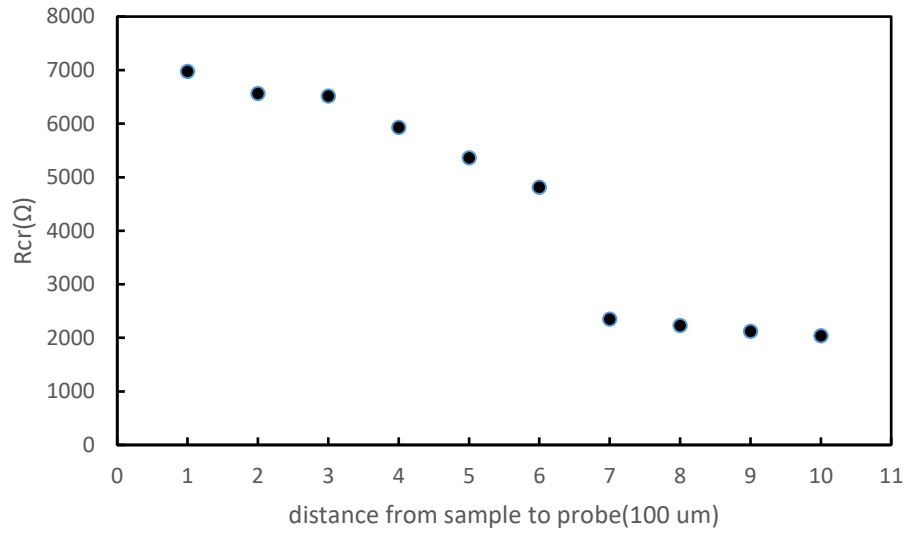
**Figure 4.4.2.9** Rcr value vs distance above Titanium sample surface (1.6 mm radius electrode )

# CHAPTER 5

# DISCUSSION AND CONCLUSION

## 5.1 The behavior of CoCrMo and Titanium sample in OCP measurements and potentiodynamic polarization test

Based on the measurements and results, the CoCrMo and Titanium samples perform similarly in the no-external-electrolyte condition. In this condition, increasing the pipette area resulted in the corrosion potential and polarization resistance for both CoCrMo and Titanium sample to decrease and the corrosion currents increased. Increased corrosion currents are to be expected as the electrode area is increased, however, it is not clear why the Ecorr changed with electrode area. This may be due to changes in the distribution of areas engaged in the oxidation and reduction half-cell reactions.

In the no-electrolyte-covered condition, the samples are only exposed to the electrolyte in the small area inside of the pipette and the changes observed are consistent with the area-dependent changes seen in electrode resistance and capacitance. With this area increasing, there are more region of the sample contacting to the electrolyte which leads to a higher density of bulk metal ion introduced. As the result the anodic reaction domains and the currents are increasing, which shifts the corrosion potential to a lower level. The polarization resistance, as determined from the polarization test, is defined as the slope of the V vs I plot at Ecorr, $R_p = \dfrac{dV}{dI}$, as the the current went up, the $R_p$ went down, as shown in figure 4.2.3 and figure 4.2.9.

However, in PBS covered condition, the Titanium sample and CoCrMo performed differently. The $E_{corr}$ of CoCrMo sample went for more negative and $R_p$ also went down along with the increasing exposing area, while the $I_{corr}$ did not change much; for Titanium sample, the value of $E_{corr}$, $I_{corr}$, and $R_p$ change was relatively small compared to the behavior in no-electrolyte-covered condition.

In the dynamic polarization tests, the $E_{corr}$ can be considered as the open circuit potential in PBS solution. Thus, based on the measurements and the results, the open circuit potential of CoCrMo alloy and Titanium samples shifted to more negative potential with the increasing pipette area in both dry/ PBS covered conditions. One possible reason for such behavior is that the OCP is the combination of the potential of oxidation reaction and reduction reaction occurring at the metal-solution interface at equilibrium. As the result the increase of the OCP is likely due to the larger density of metal ion were introduced which leads to the anodic reaction domains.

Additionally, the OCP of CoCrMo sample is more positive in the no-electrolyte condition with the same sample exposed area compared with the PBS-covered condition. This phenomenon is likely because the CoCrMo sample is more sensitive to the local PBS electrolyte attack. The higher OCP could be a result of thicker oxides film. This hypothesis can be tested in future work by using SEM or AFM to observe the structure of the very tested spot.

## 5.2 The behavior of CoCrMo and Titanium sample in Electrochemical Impedance Spectroscopy

The equivalent circuit for the no-electrolyte covered condition is a Randle's model as shown in figure 3.2. $R_s$ is the resistance of the electrolyte solution (PBS), $R_o$ is the resistance of the oxide film and $C_o$ is the capacitance of the oxide film.
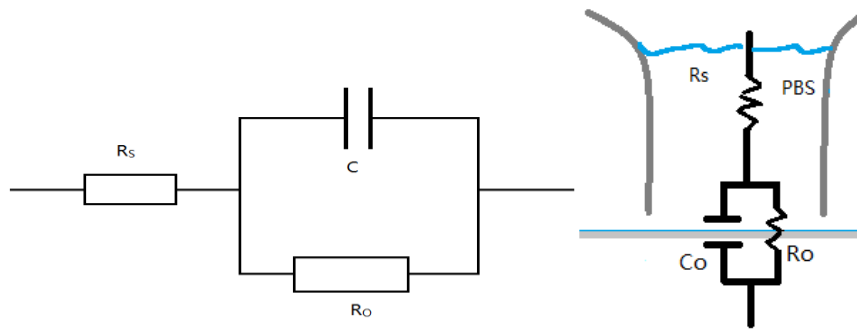


**Figure 3.2** Randle's model

Based on the measurements, in no-electrolyte-covered condition with the increasing exposed area, the CPE-T value for both CoCrMo and Titanium samples increased while the Rp value for both CoCrMo and Titanium samples decreased. As shown in figure 4.3.1.4, 4.3.1.5, 4.3.1.8 and 4.3.1.9. According to the definition of Z,

$$\frac{1}{Z} = \frac{1}{Rp} + \text{CPE-T} \ (j\omega)^{\text{CPE-P}}$$, increasing CPE-T and decreasing of $R_p$, the value of impedance would consequently decrease, as the result the impedance in a large region would be lower than a smaller area attacked by the PBS.

One reason for this phenomenon is that with increasing exposed area, more electrolyte is in contact with the metal-solution interface which leads to more oxide film generating reactions (and other reactions) causing greater total currents for the same reaction rates. Another way to understand this effects is that the resistance is defined as $R=\rho l/A$, where A is the electrode area. As the area increases, the resistance would decrease.

In the PBS-covered condition, the equivalent circuit is a crevice corrosion model as showed before in Figure 3.3. The $R_{oc}$ or external surface resistance was found to be outside of the range of the system and not measurable in the test set up.    The external capacitance, $CPE_{oc}$ was able to be measured. The crevice resistance, which arises from the junction between the pipette tip and the external solution, $R_{cr,}$ is the crevice resistance, $R_s$ is the inside electrolyte resistance, $R_o$ is the resistance of the oxide film and $CPE_o$ is the capacitance of the oxide film.
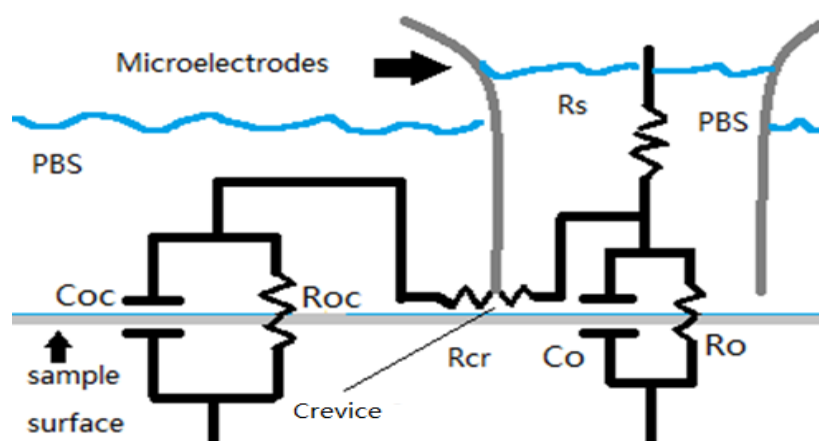


**Figure 3.3** Gilbert Crevice impedance model and the equivalent circuit

Based on the measurements, with increased pipette area, $R_o$ and $R_{cr}$ for both Titanium and CoCrMo sample are decreased while $CPE_o$ increased in an area-dependent fashion, and $CPE_{oc}$ as well as $R_{oc}$ changed relatively little compared to other parameters.

According to the model, the Ro and Co behave similarly to the no electrolyte covered condition due to the same area-dependent mechanism. The reason that Coc did not change much might be due to the fact that the outside area is fixed and is about 100 times larger than the pipette areas explored.

The impedance calculation of this model was created by Dr. Jeremy L Gilbert was implied to fit the result. The impedance in this crevice model can be calculated by following equations:

$$\tau_{oc} = R_{oc} \cdot CPEoc - T \cdot (j\omega)^{CPEoc - P}$$

$$\tau_{o} = R_{o} \cdot CPEo - T \cdot (j\omega)^{CPEo - P}$$

$$Z'_{oc} = R_{cr} + \frac{R_{oc}}{1 + (\omega\tau_{oc})^2}$$

$$Z''_{oc} = -iR_{oc}\frac{\omega\tau_{oc}}{1 + (\omega\tau_{oc})^2}$$

$$a = R_{o} + Z'_{oc} - \omega\tau_{o}Z''_{oc}$$

$$b = Z''_{oc} + \omega\tau_{o}Z'_{oc}$$

$$Z_{||} = \frac{R_{o}}{a^2 + b^2}\left[\left(Z'_{oc}\,a + Z''_{oc}\,b\right) + i\left(aZ''_{oc} - bZ'_{oc}\right)\right]$$
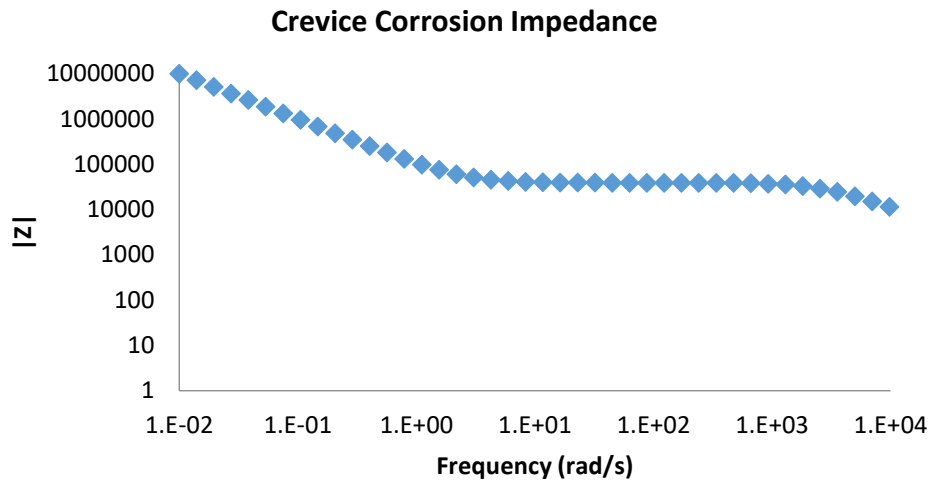
**Figure 5.2.1** Bode Plot fitting result using Gilbert Crevice Impedance equations

From right to left, the 1st plateau (far right) is dominated by Rs, and the range is dominated by Co for the left end. The 2nd plateau (in the mid-frequencies) is dominated by Rcr, and the range is determined by Co for the right end and Coc for the left end. The 3rd plat stage is dominated by whichever of Ro and Rco is smaller.

By testing and applying fitting results into the equations above, it shows that the 3rd plateau stage is dominated by Ro and Roc and is sometimes beyond the measure range. Due to the limitation of the potentiostat and the efficiency the scanning frequency cannot be lower than 0.001Hz. Thus, the value of Roc was not significant in terms of the impedance behavior observed and would not significantly influence the result once reach to $10^8$ Ω level.

Another phenomenon was found in both CoCrMo and Titanium sample tests: in PBS covered condition with the changing of the distance between the microelectrode and the sample surface, the $2^{nd}$ plateau, which is dominated by Rcr, has an exponential relationship with the distance. With the increasing distance between sample surface and the microelectrodes, the value of $2^{nd}$ plateau decreases. Also the tendency is that after a critical distance a sudden drop of Rcr occurs. This was found in every different opening size microelectrodes and in both CoCrMo and Titanium samples tests. This critical distance varies with different diameters of the pipette area and is different between CoCrMo and Titanium sample. The possible reason for this phenomenon could be that according to the resistance definition: $R= \rho l/A$, the resistance inside of the crevice is highly dependent on the gap formed and/or the tightness of the junction between the inside and outside solution regions.

This crevice model approach opens up several possibilities for the study of metallic biomaterials and implant configurations. For example, the distance between the sample surfaces to the electrodes could be equivalent to the development of the crevice between the femoral head and the femoral stem of a modular taper in a hip implant. If the reference and working electrodes could be positioned within the modular taper junction, this impedance model may be able to describe the crevice conditions for different geometries. In addition, microelectrode methods to study the internal corrosion reaction and the externally sensed corrosion reactions in the

modular taper junction may provide for new capabilities to understand the interactions between internal and external measurements.

Since the Rcr is the domain factor in the 2$^{nd}$ plateau stage with a range of 1 to 1000 Hz, this study was capable of quantitatively measuring the relationship between Rcr and the crevice height. This could help in the future of hip implant design. This phenomenon will be further studied with a more developed system with a more accurate system which be able to set the "zero" point properly and then find the accurate distances.

# Conclusions:

1. In the no-electrolyte-covered condition condition, increasing sample area affected the corrosion potential and polarization resistance for both CoCrMo and Titanium sample.   The potential decreased while the corrosion currents increased with area.

2. In the PBS-covered condition, the $E_{corr}$ of CoCrMo sample became more negative and $R_p$ also went decreased with increasing area, while the $I_{corr}$ did not change significantly. For Titanium sample, the value of $E_{corr}$, $I_{corr}$, and $R_p$ changed relatively little compared to the behavior in the no-electrolyte-covered condition.

3. In the no-electrolyte-covered condition, with increasing area, the CPE-T value for both CoCrMo and Titanium samples increased, while the Rp value for both CoCrMo and Titanium sample decreased.

4. In the PBS-covered condition, with increasing pipette area, $R_o$ and $R_{cr}$ for both Titanium and CoCrMo samples decreased while $CPE_o$ increased, and $CPE_{oc}$ as well as $R_{oc}$ changed relatively little compared to other parameters.

5. In the PBS-covered condition, with changes in the pipette-electrode surface distance, Rcr has a inverse relationship with distance. And there is a critical

distance which leads to a sudden Rcr value drop most likely due to direct contact

between the pipette tip and the surface.

# CHAPTER 6

# TECHNICAL DESIGN ASSESSMENT AND FUTURE WORK

The goal of this study was to develop a microelectrode system capable of sampling small regions (or controlling the detected area size) to identify and quantitatively measure the variations in electrochemical properties. With systemically and functionally performing electrochemical measurements such as OCP test, potentiodynamic polarization test and EIS on Titanium and CoCrMo samples, this technique has shown great potential to be further developed and applied to other tests and configurations.

For aim 1, a shortfall of the current setup is the sample geometry. The sample holder can only contain a sheet or short tube like specimen while the variation of the sample geometries requires not only different shapes of the holder but also suitable microelectrodes probe design. For future work, more sample holders and fitting probes will be developed to allow this system to perform localized electrochemical measurements on different types of samples.

For aim 2, the system performed well for localized electrochemical measurement. The relationship between pipette area and electrochemical characteristics such as $E_{corr}$, $I_{corr}$, and $R_p$, etc. had been qualitatively studied. However, how would other parameters such as the distance between electrodes and the sample surface, the distance between the electrodes influence the local electrochemical behavior remains unknown. For the next stage, the quantitative

relationship between the explored factors will be studied, and the unexplored factors stated above will be studied as well.

Additionally, the crevice model approach opens up several possibilities for the study of metallic biomaterials and implant configurations. For example, the distance between the sample surfaces to the electrodes could be equivalent to the development of the crevice between the femoral head and the femoral stem of a modular taper in a hip implant. If the reference and working electrodes could be positioned within the modular taper junction, this impedance model may be able to describe the crevice conditions for different geometries. In addition, microelectrode methods to study the internal corrosion reaction and the externally sensed corrosion reactions in the modular taper junction may provide for new capabilities to understand the interactions between internal and external measurements.

In future, experiments to assess pre- and post-corrosion tested sample surface structure can be performed to identify and characterize the local structural heterogeneities giving rise to the differing electrochemical responses. A visualizing tool such as SEM, AFM and optical digital microscope will be applied to characterize the structure and defect distribution (size and location) within samples prior to testing and afterward to correlate where electrochemical changes are detected to any observable structural variations (defects, inclusions, grain boundaries) change the

local electrochemical behavior will be analyzed and corresponded to the actual

sample surface structure.

# References

[1]     A. Matthies, R. Underwood, P. Cann, K. Ilo, Z. Nawaz, J. Skinner*, et al.*, "Retrieval analysis of 240 metal-on-metal hip components, comparing modular total hip replacement with hip resurfacing," *Bone & Joint Journal,* vol. 93-B, pp. 307-314, 2011-03-01 00:00:00 2011.

[2]     J. L. Gilbert, S. Mali, R. M. Urban, C. D. Silverton, and J. J. Jacobs, "In vivo oxide-induced stress corrosion cracking of Ti-6Al-4V in a neck–stem modular taper: Emergent behavior in a new mechanism of in vivo corrosion," *Journal of Biomedical Materials Research Part B: Applied Biomaterials,* vol. 100B, pp. 584-594, 2012.

[3]     G. B. Higgs, J. A. Hanzlik, D. W. MacDonald, W. M. Kane, J. S. Day, G. R. Klein*, et al.*, "Method of Characterizing Fretting and Corrosion at the Various Taper Connections of Retrieved Modular Components from Metal-on-Metal Total Hip Arthroplasty," pp. 146-156, 2013.

[4]     R. Pivec, R. M. Meneghini, W. J. Hozack, G. H. Westrich, and M. A. Mont, "Modular Taper Junction Corrosion and Failure: How to Approach a Recalled Total Hip Arthroplasty Implant," *The Journal of Arthroplasty,* vol. 29, pp. 1-6, 1// 2014.

[5]     G. Gkagkalis, P. Mettraux, P. Omoumi, S. Mischler, and H. A. Rüdiger, "Adverse tissue reaction to corrosion at the neck-stem junction after modular primary total hip arthroplasty," *Orthopaedics & Traumatology: Surgery & Research,* vol. 101, pp. 123-126, 2// 2015.

[6]     Y.-M. Kwon, S. Glyn-Jones, D. J. Simpson, A. Kamali, P. McLardy-Smith, H. S. Gill*, et al.*, "Analysis of wear of retrieved metal-on-metal hip resurfacing implants revised due to pseudotumours," *Bone & Joint Journal,* vol. 92-B, pp. 356-361, 2010-03-01 00:00:00 2010.

[7]     M. Paliwal, D. G. Allan, and P. Filip, "Retrieval Analysis of a Cementless Modular Total Hip Arthroplasty Prosthesis," in *2007 IEEE 7th International Symposium on BioInformatics and BioEngineering*, 2007, pp. 553-558.

[8]     H.-P. Sieber, C. B. Rieker, and P. Köttig, "Analysis of 118 second-generation metal-on-metal retrieved hip implants," *Bone & Joint Journal,* vol. 81-B, pp. 46-50, 1999-01-01 00:00:00 1999.

[9]     J. J. JACOBS, J. L. GILBERT, and R. M. URBAN, "Current Concepts Review - Corrosion of Metal Orthopaedic Implants*," *The Journal of Bone & Joint Surgery,* vol. 80, pp. 268-82, 1998-02-01 00:00:00 1998.

[10]    D. C. Rodrigues, R. M. Urban, J. J. Jacobs, and J. L. Gilbert, "In vivo severe corrosion and hydrogen embrittlement of retrieved modular body titanium alloy hip-implants," *Journal of Biomedical Materials Research Part B: Applied Biomaterials,* vol. 88B, pp. 206-219, 2009.

[11]    J. L. Gilbert, M. Mehta, and B. Pinder, "Fretting crevice corrosion of stainless steel stem–CoCr femoral head connections: Comparisons of

materials, initial moisture, and offset length," *Journal of Biomedical Materials Research Part B: Applied Biomaterials,* vol. 88B, pp. 162-173, 2009.

[12] S. A. Brown, C. A. C. Flemming, J. S. Kawalec, H. E. Placko, C. Vassaux, K. Merritt*, et al.*, "Fretting corrosion accelerates crevice corrosion of modular hip tapers," *Journal of Applied Biomaterials,* vol. 6, pp. 19-26, 1995.

[13] F. Amerstorfer, S. F. Fischerauer, L. Fischer, J. Eichler, J. Draxler, A. Zitek*, et al.*, "Long-term in vivo degradation behavior and near-implant distribution of resorbed elements for magnesium alloys WZ21 and ZX50," *Acta Biomaterialia.*

[14] A. H. Hosman, H. C. van der Mei, S. K. Bulstra, H. J. Busscher, and D. Neut, "Effects of metal-on-metal wear on the host immune system and infection in hip arthroplasty," *Acta Orthopaedica,* vol. 81, pp. 526-534, 10/08 02/01/received 04/23/accepted 2010.

[15] J. L. Gilbert, C. A. Buckley, and J. J. Jacobs, "In vivo corrosion of modular hip prosthesis components in mixed and similar metal combinations. The effect of crevice, stress, motion, and alloy coupling," *Journal of Biomedical Materials Research,* vol. 27, pp. 1533-1544, 1993.

[16] V. Swaminathan and J. L. Gilbert, "Fretting corrosion of CoCrMo and Ti6Al4V interfaces," *Biomaterials,* vol. 33, pp. 5487-5503, 8// 2012.

[17] G. M. Keegan, I. D. Learmonth, and C. P. Case, "Orthopaedic metals and their potential toxicity in the arthroplasty patient," *A REVIEW OF CURRENT KNOWLEDGE AND FUTURE STRATEGIES,* vol. 89-B, pp. 567-573, 2007-05-01 00:00:00 2007.

[18] A. K. Madl, M. Kovochich, M. Liong, B. L. Finley, D. J. Paustenbach, and G. Oberdörster, "Toxicology of wear particles of cobalt-chromium alloy metal-on-metal hip implants Part II: Importance of physicochemical properties and dose in animal and in vitro studies as a basis for risk assessment," *Nanomedicine: Nanotechnology, Biology and Medicine,* vol. 11, pp. 1285-1298.

[19] S. J. Stohs and D. Bagchi, "Oxidative mechanisms in the toxicity of metal ions," *Free Radical Biology and Medicine,* vol. 18, pp. 321-336, 1995/02/01 1995.

[20] H. Baba, T. Kodama, and Y. Katada, "Role of nitrogen on the corrosion behavior of austenitic stainless steels," *Corrosion Science,* vol. 44, pp. 2393-2407, 10// 2002.

[21] H.-H. Huang, "Effect of chemical composition on the corrosion behavior of Ni-Cr-Mo dental casting alloys," *Journal of Biomedical Materials Research,* vol. 60, pp. 458-465, 2002.

[22] B. A. Kehler, G. O. Ilevbare, and J. R. Scully, "Crevice Corrosion Stabilization and Repassivation Behavior of Alloy 625 and Alloy 22," *CORROSION,* vol. 57, pp. 1042-1065, 2001.

[23] A. Pardo, E. Otero, M. C. Merino, M. D. López, M. V. Utrilla, and F. Moreno, "Influence of pH and Chloride Concentration on the Pitting and Crevice Corrosion Behavior of High-Alloy Stainless Steels," *CORROSION,* vol. 56, pp. 411-418, 2000/04/01 2000.

[24] B. E. Wilde and E. Williams, "The Relevance of Accelerated Electrochemical Pitting Tests to the Long‐Term Pitting and Crevice Corrosion Behavior of Stainless Steels in Marine Environments," *Journal of The Electrochemical Society,* vol. 118, pp. 1057-1062, July 1, 1971 1971.

[25] J. Gilbert, "Prevention of fretting crevice corrosion of modular taper interfaces in orthopedic implants," ed: Google Patents, 2014.

[26] A. H. Deutchman, R. J. Partyka, and R. J. Borel, "Orthopaedic implants having self-lubricated articulating surfaces designed to reduce wear, corrosion, and ion leaching," ed: Google Patents, 2008.

[27] G. Kappelt, P. Kurze, and D. Banerjee, "Method for producing a corrosion-inhibiting coating on an implant made of a bio-corrodible magnesium alloy and implant produced according to the method," ed: Google Patents, 2008.

[28] L. Tang, "Nanocoating for improving biocompatibility of medical implants," ed: Google Patents, 2005.

[29] F. A. España, V. K. Balla, S. Bose, and A. Bandyopadhyay, "Design and fabrication of CoCrMo alloy based novel structures for load bearing implants using laser engineered net shaping," *Materials Science and Engineering: C,* vol. 30, pp. 50-57, 1/1/ 2010.

[30] S.-M. Park and J.-S. Yoo, "Peer Reviewed: Electrochemical Impedance Spectroscopy for Better Electrochemical Measurements," *Analytical Chemistry,* vol. 75, pp. 455 A-461 A, 2003/11/01 2003.

[31] D. D. Macdonald, "Reflections on the history of electrochemical impedance spectroscopy," *Electrochimica Acta,* vol. 51, pp. 1376-1388, 1/20/ 2006.

[32] L. G. Jeremy, A. M. Sachin, and L. Yangping, "Area-dependent impedance-based voltage shifts during tribocorrosion of Ti-6Al-4V biomaterials: theory and experiment," *Surface Topography: Metrology and Properties,* vol. 4, p. 034002, 2016.

[33] I. Annergren, D. Thierry, and F. Zou, "Localized Electrochemical Impedance Spectroscopy for Studying Pitting Corrosion on Stainless Steels," *Journal of The Electrochemical Society,* vol. 144, pp. 1208-1215, April 1, 1997 1997.

[34] F. Zou and D. Thierry, "Electrochemical Microsystem TechnologiesLocalized electrochemical impedance spectroscopy for studying the degradation of organic coatings," *Electrochimica Acta,* vol. 42, pp. 3293-3301, 1997/01/01 1997.

[35] F. Zou, D. Thierry, and H. S. Isaacs, "A High‐Resolution Probe for Localized Electrochemical Impedance Spectroscopy Measurements," *Journal of The Electrochemical Society,* vol. 144, pp. 1957-1965, June 1, 1997 1997.

[36] A. W. Hassel and M. M. Lohrengel, "Electrochemical Microsystem TechnologiesThe scanning droplet cell and its application to structured nanometer oxide films on aluminium," *Electrochimica Acta,* vol. 42, pp. 3327-3333, 1997/01/01 1997.

[37] I. M. Zin, S. B. Lyon, and A. Hussain, "Under-film corrosion of epoxy-coated galvanised steel: An EIS and SVET study of the effect of inhibition at defects," *Progress in Organic Coatings,* vol. 52, pp. 126-135, 2/1/ 2005.

[38] M. Gębala, W. Schuhmann, and F. La Mantia, "A new AC-SECM mode: On the way to high-resolution local impedance measurements in SECM," *Electrochemistry Communications,* vol. 13, pp. 689-693, 7// 2011.

[39] M. T. Ehrensberger and J. L. Gilbert, "A time-based potential step analysis of electrochemical impedance incorporating a constant phase element: A study of commercially pure titanium in phosphate buffered saline," *Journal of Biomedical Materials Research Part A,* vol. 93A, pp. 576-584, 2010.

# Vita

**Name of Author**: Sile Hu

**Date of Birth**: Apr. 26, 1990

**Mobile**: (+1) 315 382 9018

**Email Address**: shu13@syr.edu

## Education Background

09/2009-07/2013, Biomedical Engineering, School of Life Science and Technology,

Jinan University, Bachelor of Engineering.

09/2013-present, Bioengineering, College of Engineering and Computer Science,

Syracuse University, Master of Engineering

## Skills:

3 years' biomedical laboratory experience, familiar with operating most of instruments

on material physical and electrochemical property analysis

General computer skills, familiar with software like MS Office, Labview, Zplot,

Corrware, Makerbot, etc. Basic understanding of programming with C++

Familiar with general medical diagnose equipment's concept like MRI, CT, X-ray, etc.

Professional English and Chinese writing and oral skill

**Internship**

08/2012-10/2012, Affiliated Hospital of Inner Mongolia Medical University. Learnt to operate medical detection machines like color Doppler ultrasonic detector, etc. Collected the case reports and analyzed the detection reports. Cooperated with other interns on helping patients with reservation, medical inspection and submit detection reports.

05/2012-08/2012, Guangdong Artificial Limb Center. Practiced to make inner pad of lower limbs with sponge and silica gel and participated in the outer holder of lower limbs with gauze and glass fiber preparation.